RESULTS AND DISCUSSION

4.1 Isolation and identification of indigenous microalgae

4.1.1 Microalgae isolation from various sources

Initially, seven microalgae strains were isolated using BBM media supplemented with agar. The microalgae were identified by morphological analysis with bright field microscopy. The single colonies of microalgae were spread on petri plates as shown in Figure 4.1. Isolated microalgae were found to belong to the family of *Chlorellaceae*, *Scenedesmaceae*, and *Chlamydomonadaceae*. The microscopic views of all the seven microalgae are shown in Figure 4.2. The microalgae were given code based on their source, i.e. R1, R2 and R3 from isolated from Ravidas ghat; D1 and D2 isolated from Durgakund pond; B1 and B2 isolated from BHU pond.

4.1.2 The selection of isolated microalgae

The analysis of carbohydrate content, starch content, lipid content and biomass concentration of several isolated microalgae were performed, and the results are shown in Table 4.1. The microalgae R1 and D1 contain high carbohydrate content compared to others isolated microalgae, i.e., 34.0 % and 39.4% respectively. The biomass concentration was found as 1.25g/L and 1.15 g/L for R1 and D1 microalgae respectively. Based on the high carbohydrate content, two microalgae R1 and D1 were chosen as a substrate for the production of bioethanol.

Two of the isolated strains R1 and D1 were selected for further studies because of their two superior properties. First, they can grow in wastewater and second, they can accumulate high carbohydrate content. One of the two strains had similar morphological features as *Chlorella*

sp. The genus Chlorella is placed in the member of the family Chlorellaceae and is a genus of single-celled green algae with a spherical, globular or ellipsoidal shape and a cell size of about 2–10 μm. The cells are devoid of flagella, having a parietal and cup-shaped chloroplast with a single pyrenoid surrounded by a thin cellulose wall.

The morphological features of second isolated strain resemble that of genus *Scenedesmus*, which belongs to the family Scenedesmaceae within the class Chlorophyceae. The observed cells are small, non-motile, cylindrical, elongated or fusiform in shape with pointed ends. The colonies are usually observed in groups of two or four spindle-shaped cells aligned laterally with the curved outer side. Cells are approximately 2–6 μm wide and 9–30μm long. Each cell contains a chloroplast with a pyrenoid and lacks the presence of spines.

The molecular characterisation of R1 and D1 were further performed by extracting the genomic DNA and PCR amplification of the conserved regions. PCR amplicons were sequenced and compared with other microalgae.

4.1.3 PCR amplification and sequencing of ITS and 5.8S rRNA genes and phylogenetic analysis

The isolated total DNA was applied as potential markers for species identification by PCR amplification of the ITS and 5.8S rRNA gene sequence. Two bands of amplified ITS and 5.8S rRNA gene sequence as shown in Figure 4.3 with a size of 330 bp and 252 bp were successfully obtained from strain R1 and D1 respectively. BLAST homology analysis yielded close matches of these sequences with ITS and 5.8S rRNA gene region of *C. sorokiniana* and *T. obliquus* respectively. The BLAST analysis for both the microalgae R1 and D1 was performed and a Neighbor-Joining (NJ) tree based on the nucleotide sequences was constructed with MEGA 6.0 software as shown in Figure 4.4. The result showed that

these two strains belong to *C. sorokiniana* and *T. obliquus*, with bootstrap support of 100%, with the closest similarity to the *C. sorokiniana* isolate CFR 3-05/FW (KU695583) and *Tetradesmus* sp. NEIST BT-A10 (MG799371) respectively.

Table 4.1: The composition of isolated microalgae

S. No.	Code	Microalgae	Biomass (g/L)	Carbohydrate content % (w/w), (mean ± sd)	Starch content % (w/w), (mean ± sd)	Lipid content (w/w), (mean ± sd)
1	R1	*Chlorella sp*	1.25	34.0±0.6	20.7±0.3	25.4±0.5
2	R2	*Chlorella sp.*	1.18	22.7±0.4	13.58±0.5	23.1±0.5
3	R3	*Nanocloropsis sp.*	0.98	18.5±0.4	11.2±0.7	25.2±0.6
4	D1	*Tetradesmus sp.*	1.15	39.4±1.3	23.9±0.2	21.5±0.7
5	D2	*Scenedesmus sp.*	1.13	19.3±0.5	11.8±0.4	26.0±0.8
6	B1	*Chlamydomonas sp.*	1.01	31.4±0.7	18.8±0.8	19.2±0.6
7	B2	*Chlorella sp.*	1.09	26.5±0.8	16.2±0.7	18.3±0.4

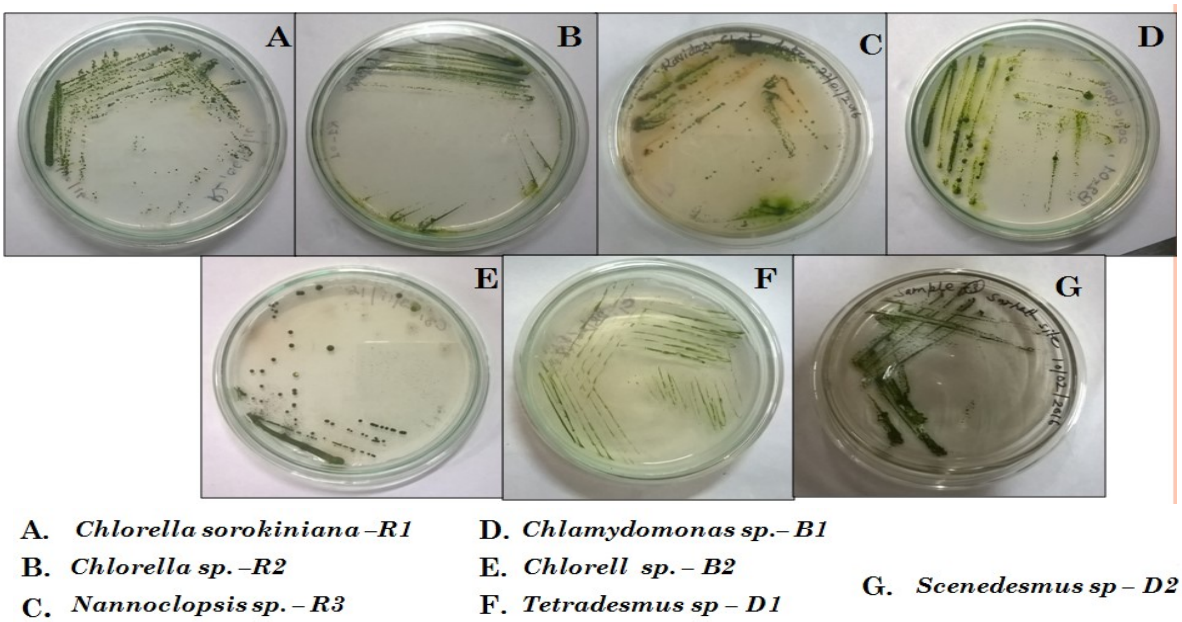

Fig. 4.1: Pure colonies of isolated microalgae

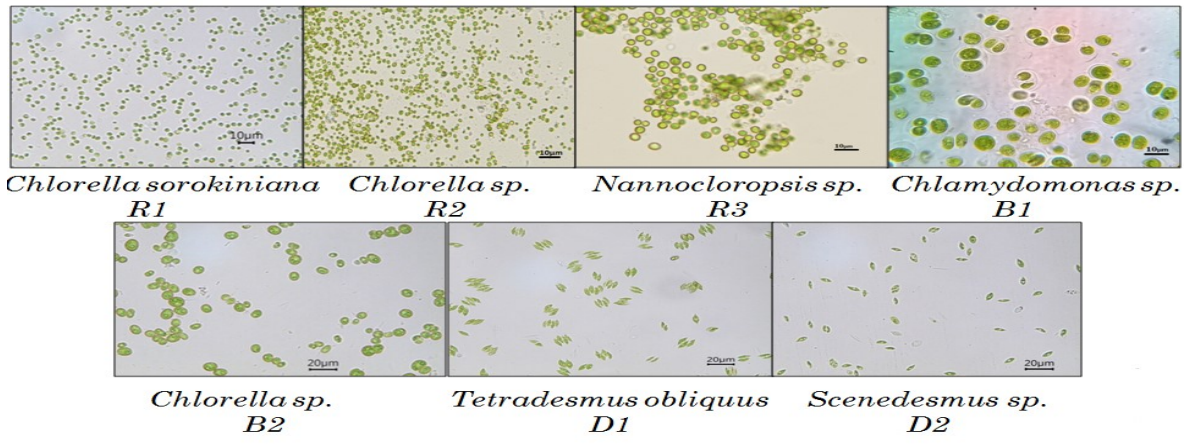

Fig. 4.2: Microscopic view of isolated microalgae

4.1.4 Partial sequences of ITS and 5.8s rRNA gene of isolated microalgae

DNA were isolated from both microalgae and were subjected to amplification using PCR. The purified DNA was then sequenced using an automated sequencer. The partial gene sequences of both microalgae were then submitted at National Center for Biotechnology Information (NCBI). Following are the sequences of both the microalgae along with the accession numbers (shown in bracket):

R1-Chlorella sorokiniana (KY348331)

AGTACGACGATCACCCTGGCACTACCCCGTCCCCTCGCGCGGTCCCCACCTGGCC
ATCGCCGGCCGGTGGGGGCAGCGAGCGCCGTGTTCCTTGGCGGGGCTCTCCGGA
GCGCCGCCTGGGTCCGGCGGGCGTCCCTCCACATGCGCGGCCTCGGTCGCCTTGG
GAGGAGAAGCGCTGGCAAATCCTTGTATCCAACCCCAATTTCACTCCAAACCTG
AACGTCAGCTGAAGCACCTTGCGCCCCGAGCATGCCTCGGCCGCAATCAAAACC
AACGACAACTCTCAACAACGGATATCTTGGCTCCCGCATCGATGAAGAACGCAG
CAAT

D1- Tetradesmus obliquus IIT-BHU BC01 (*MH045839*)

CCAATGCTGCACCATATCTGTTCCGTGCCTTAGCTGCCAGCAAGGCAATTGGGCT
TTGCCTGATGTACTTGCAAGCTGGTGCGAGTAATTTTTACTTGCATCAGTGGCGC
TCTGGCATGCTTATACACCAGTGCTAACCACTGTCAAAACCAAACTCTGAAGCTA
TGATTGCTATTAATTGGCAATCTTAACCAAAGA

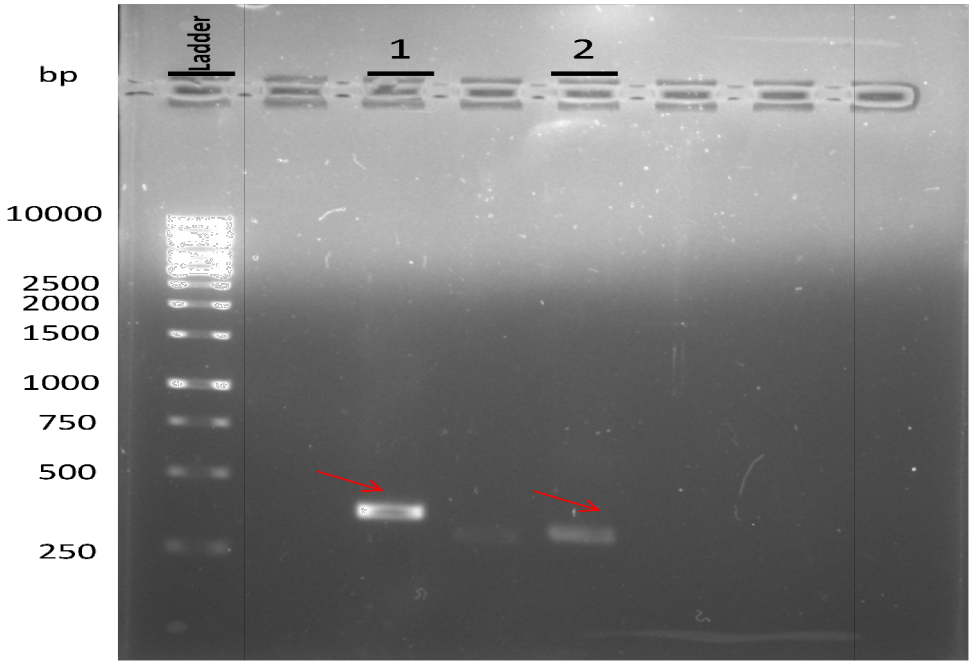

Fig. 4.3: Agarose gel electrophoresis of PCR Amplified 5.8s rRNA gene
(Well no.1 contains R1 and well no. 2 contains D1)

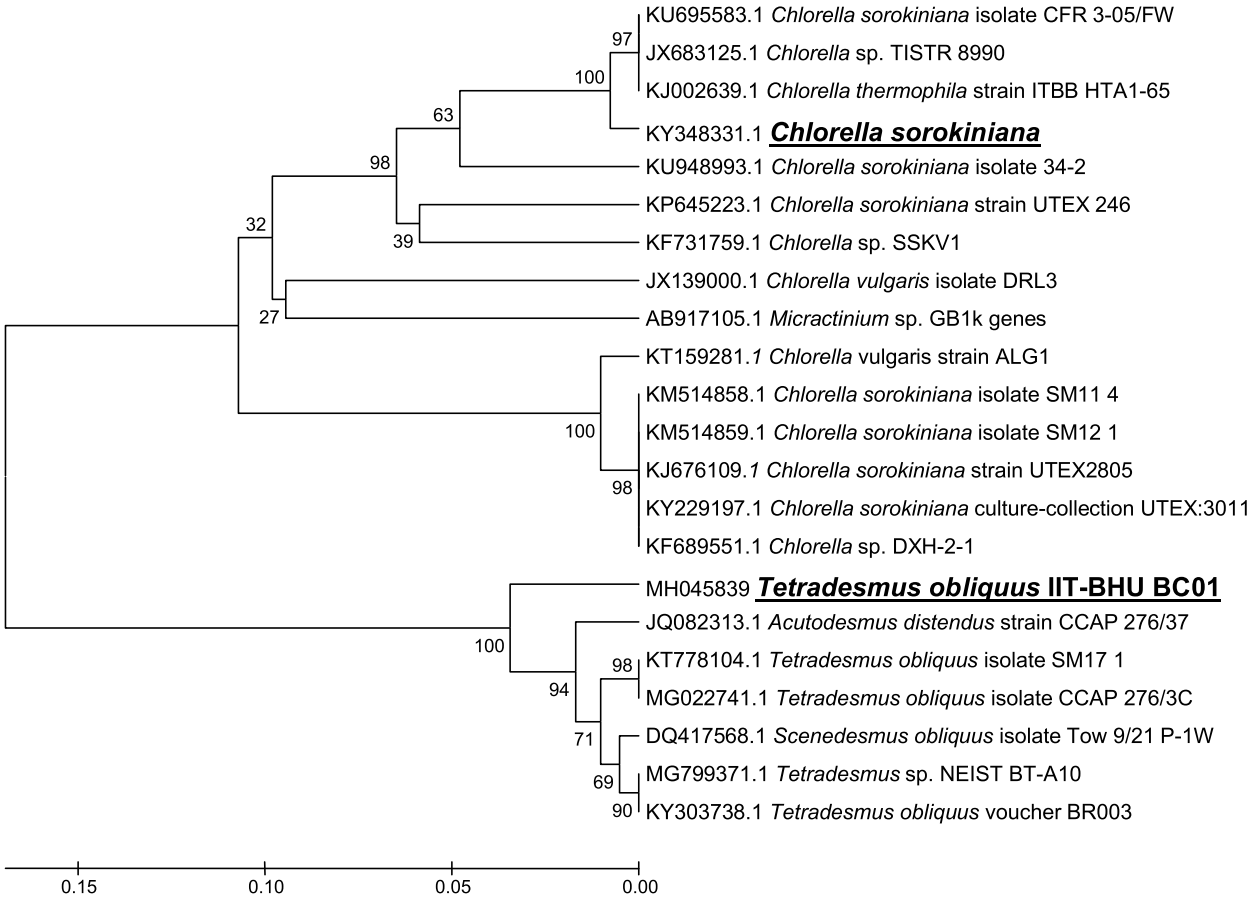

Fig 4.4: Maximum likelihood phylogenetic tree of 18s rRNA sequence of isolated microalgae (Numbers above branches show the bootstrap values of maximum likelihood analysis from 1000 replicates)

4.2 Growth study of microalgae in different culture conditions

4.2.1 Effect of inoculum size and media composition on microalgae growth

The microalgae *C. sorokiniana* and *T. obliquus* were grown with different inoculum sizes (0.5%, 2% and 5% v/v) having average cell density about 10^8 cells /mL in three different growth media, *i.e.* BG11, BBM and CHU M10. The effect of different inoculums sizes i.e. 0.5%, 2% and 5% v/v are shown in Figure 4.5, 4.6 and 4.7 respectively. The experimental

results show that high inoculum size was more favourable for the microalgae growth and higher biomass production obtained as compared to small inoculum size. Also, it was observed that in the same growth media, a large inoculum size minimised the arrival time to reach the stationary phase.

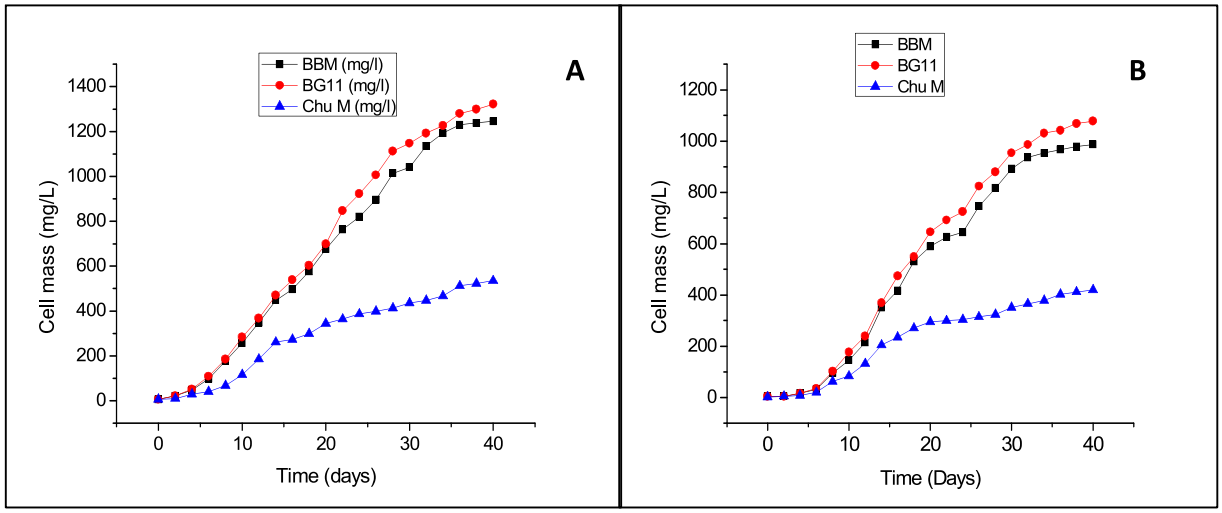

Fig. 4.5: Growth of *C. sorokiniana* (A) and *T. obliquus* (B) with 0.5 % (v/v) inoculum

The growth rates of both the microalgae were found significantly higher in BG11 and BBM media compared to CHU M10 media. The maximum biomass production for both the microalgae was found in BG11 media with all three different inoculum sizes of microalgae, *C. sorokinaina,* and *T. obliquus*. Therefore, BG11 were chosen as growth media for further studies. Figure 4.5 shows the effect of 0.5 % inoculums (V/V) on the growth of *C. sorokiniana* (Figure 4.5 A) and *T. obliquus* (Figure 4.5 B) grown in BG11, BBM and CHU M10 media. The biomass concentrations obtained with 0.5% inoculum size were 1322 mg/L and 1078 mg/L in BG11 media, 1246 mg/L and 987 mg/L in BBM media, and 536 mg/L and 420 mg/L in CHU10 media for *C. sorokiniana* and *T. obliquus* respectively.

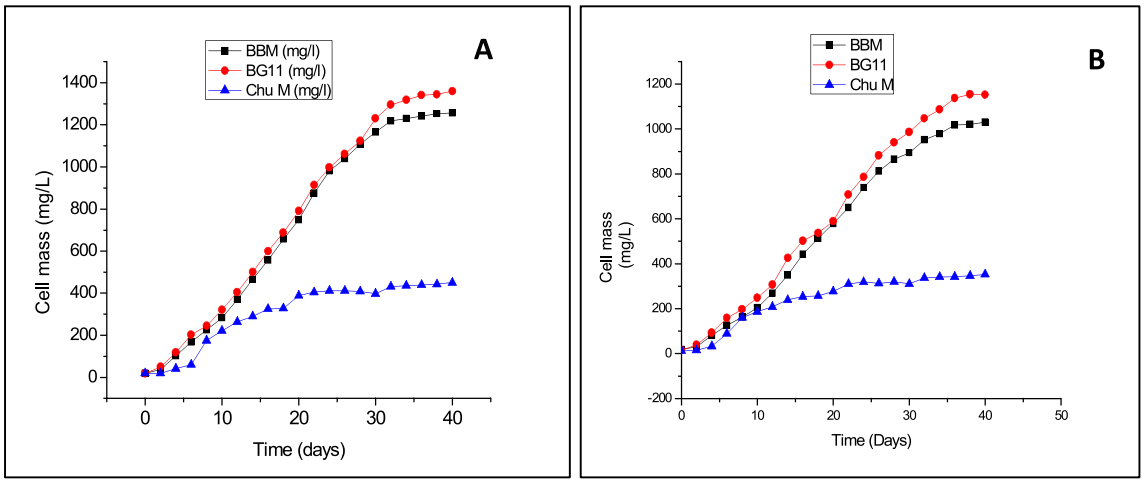

Fig.4.6: Growth of *C. sorokiniana* (A) and *T. obliquus* (B) with 2.0 % (v/v) inoculum

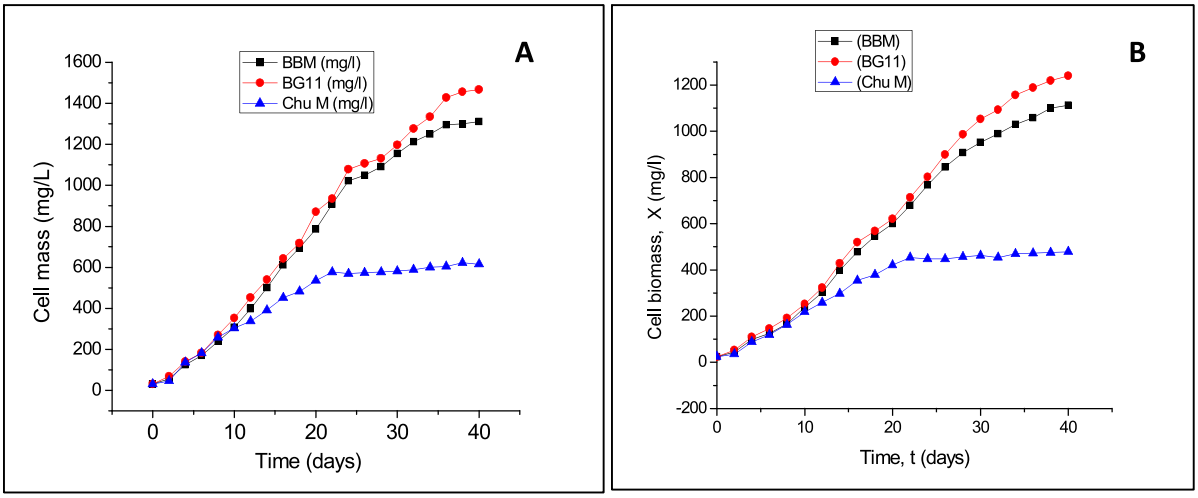

Fig. 4.7: Growth of *C. sorokiniana* (A) and *T. obliquus* (B) with 5.0 % (v/v) inoculum

Figure 4.6 shows the growth profile of *C. sorokiniana* (4.6 A) and *T. obliquus* (4.6 B) with 2% of inoculum. The microalgae cell mass concentrations were 1360 mg/L and 1152 mg/L in BG11 media, 1257 mg/L and 1030 mg/L in BBM media, and 451 mg/L and 353 mg/L in CHU M10 media for *C. sorokiniana* and *T. obliquus* respectively. Figure 4.7 shows the growth curve of microalgae *C. sorokiniana* (4.7 A) and *T. obliquus* (4.7 B) with 5% of inoculum which resulted in the highest biomass production. Cell mass concentrations obtained with 5% inoculum size were 1467 mg/L and 1240 mg/L in BG11 media, 1311 mg/L

and 1112 mg/L in BBM media, and 616 mg/L and 483 mg/L in CHU M10 media for *C. sorokiniana* and *T. obliquus* respectively. It was observed in the study that as the size of inoculums was increased, the lag phase of the growth curve was decreased. Therefore, the higher the inoculum size favours the biomass production by reducing the cultivation time.

4.2.2 Effect of initial pH

The variations in the growth of microalgae at different initial pH values were also studied. The effect of initial pH on the growth of microalgae, *C. sorokiniana,* and *T. obliquus* is shown in Figure 4.8. The results show that the variation of initial pH from pH 6.0 to 8.0 does not affect the growth of *C. sorokiniana* very much. However, at pH 7.5 the growth of *C. sorokiniana* was maximum. The growth of *T. obliquus* was also not affected by the variation of initial pH from 6.0 to 8.0. Therefore pH 7.5 was used for further studies for both the microalgae.

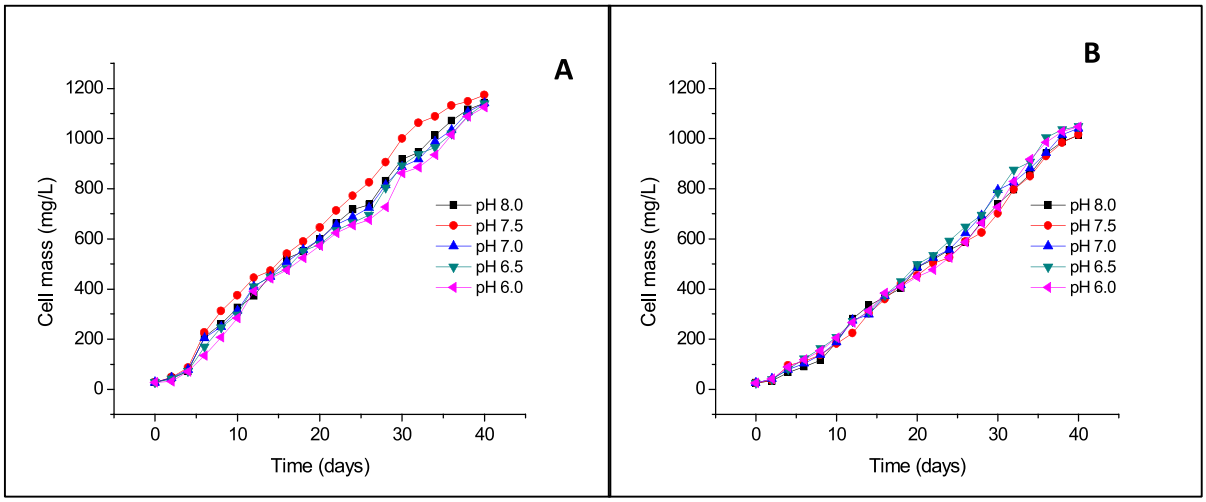

Fig. 4.8: Growth of *C. sorokiniana* (A) and *T. obliquus* (B) at different pH

4.2.3 Effect of temperature

Microalgae, *C. sorokiniana,* and *T. obliquus* were grown in BG11 media at different temperatures. The effect of temperature variations on the specific growth rates are shown in Figure 4.9 (data significant at $p < 0.05$). As temperature was increased from 20°C to 30°C, the

specific growth rate (μ) of *C. sorokiniana* increased from 0.196 day^{-1} to 0.224 day^{-1}, but as the temperature was further increased up to 40 °C, growth decreased to 0.175 day^{-1}. Similarly in case of *T. obliquus*, as the temperature was increased from 20°C to 25°C, the specific growth rate (μ) of *T. obliquus* increased from 0.203 day^{-1} to 0.221 day^{-1} whereas a further increase in temperature reduced the growth rate which reached to 0.169 day^{-1} at 40°C. The optimum temperatures for growth of *C. sorokiniana* and *T. obliquus* were observed as 30°C and 25°C respectively. The statistical analysis was performed and p-value<0.05 was obtained.

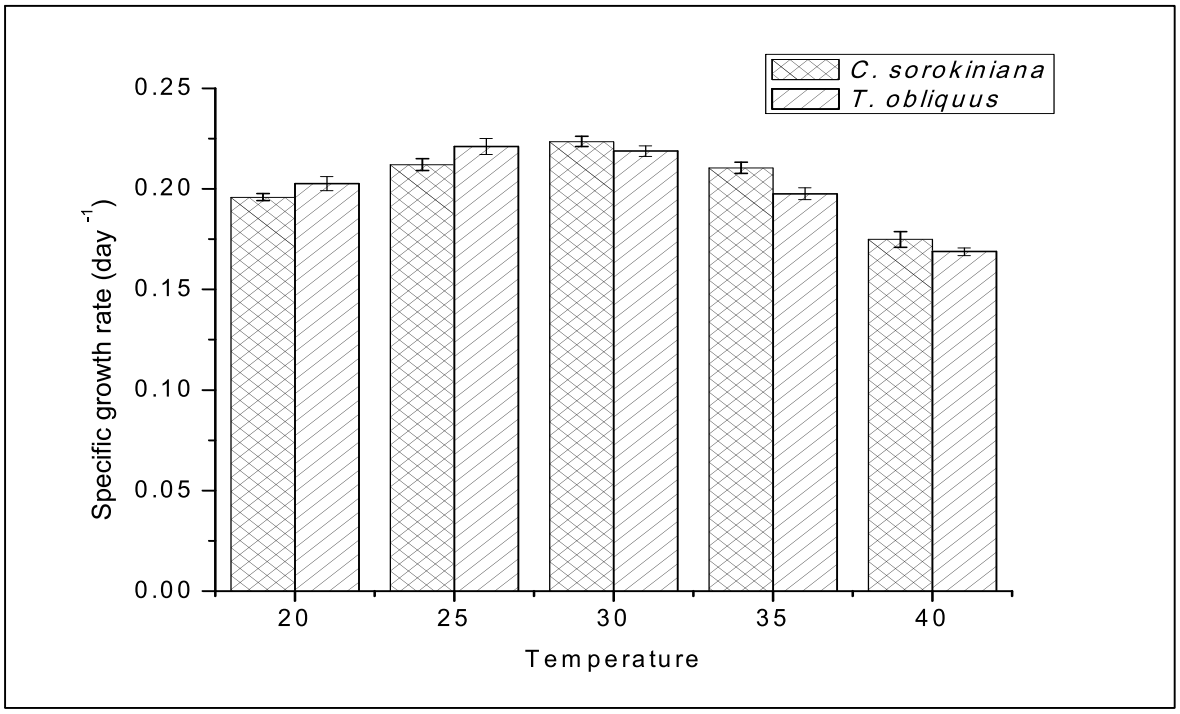

Fig. 4.9: Specific growth rates of *C. sorokiniana* and *T. obliquus* at different temperatures

4.2.4 Effect of agitation

The microalgae were grown in BG11 media in autotrophic conditions at 30°C and different agitation rates. The effect of agitation rate on microalgae growth is shown in Figure 4.10 (a) (*C. sorokiniana*) and Figure 4.10 (b) (*T. obliquus*). The microalgae were grown at the non-agitated (stationary) condition and different agitation rates, i.e., 90 rpm to 150 rpm. The biomass concentrations at non-agitated condition were observed as 1158 mg/L and 1050

mg/L for *C. sorokiniana* and *T. obliquus* respectively. The highest biomass concentrations in shake flask study were obtained with 150 rpm as 1618 mg/L and 1321 mg/L for *C. sorokiniana* and *T. obliquus* respectively. Therefore, it was concluded from the study that the increase in agitation rate in a shake flask study positively affected the growth rate of microalgae and also increased the biomass production. The reason for higher growth rate may be due to increased mass transfer of gases and nutrients. Yusuf *et al.* also reported that the increase in agitation rate from 100 rpm to 400 rpm increased the biomass production of microalgae, *Aurantiochytrium sp.*from 6.7 g/L to 20.6 g/L under heterotrophic conditions (Nazir et al., 2018).

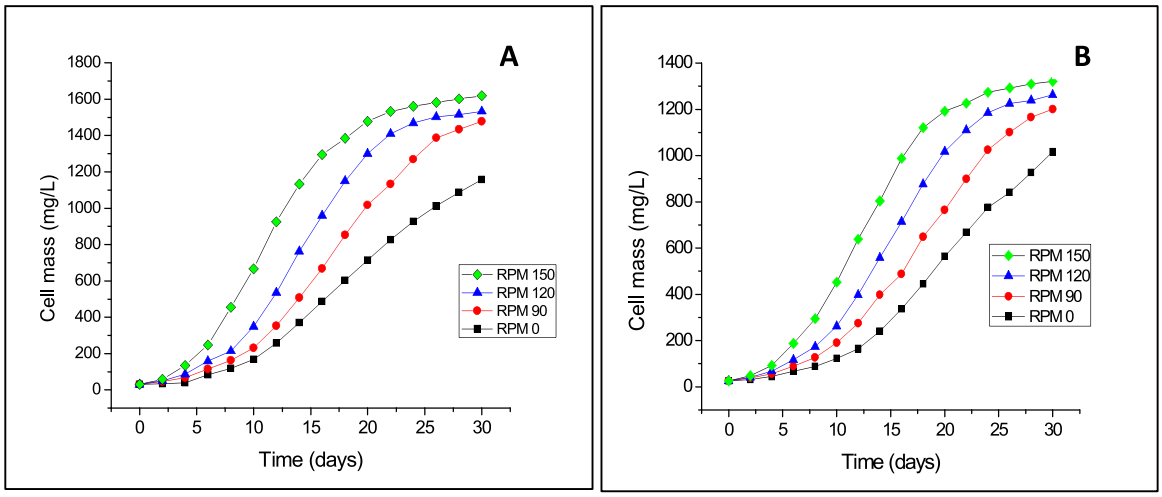

Fig. 4.10: Growth of *C. sorokiniana* (a) and *T. obliquus* (b) at different agitation conditions

4.2.5 Growth study of microalgae in different photobioreactors

Since the carbohydrate content of the microalgae is directly correlated with biomass production. Therefore, it is necessary to measure the growth yield of microalgae in different photobioreactors. Microalgae were grown in BG11 media using different photobioreactors like bubble column, stirrer tank, internal-loop airlift, and external-loop airlift photobioreactors to achieve a higher yield of algal biomass.

4.2.5.1 Growth study of microalgae in bubble column photobioreactor (BCPBR)

The growth of microalgae in bubble column photobioreactor is shown in Figure 4.11. The change in colour from light green to dark green shows the microalgal growth. The growth profiles of microalgae with air and 2% CO_2 were measured and shown in Figure 4.12 (*C. sorokiniana* (a) and *T. obliquus* (b)). *C. sorokiniana* and *T. obliquus* were grown at 30°C and 25°C respectively at an initial pH of 7.5 in BG11 media. Microalgae utilise the CO_2 and fix it as carbohydrate or lipid by photosynthesis. In another experiment, it was found that 2% CO_2 was the optimum concentration because the further increase in CO_2 concentration above 2% reduced the pH of the medium and decreased the microalgal growth (Singh and Singh, 2014).

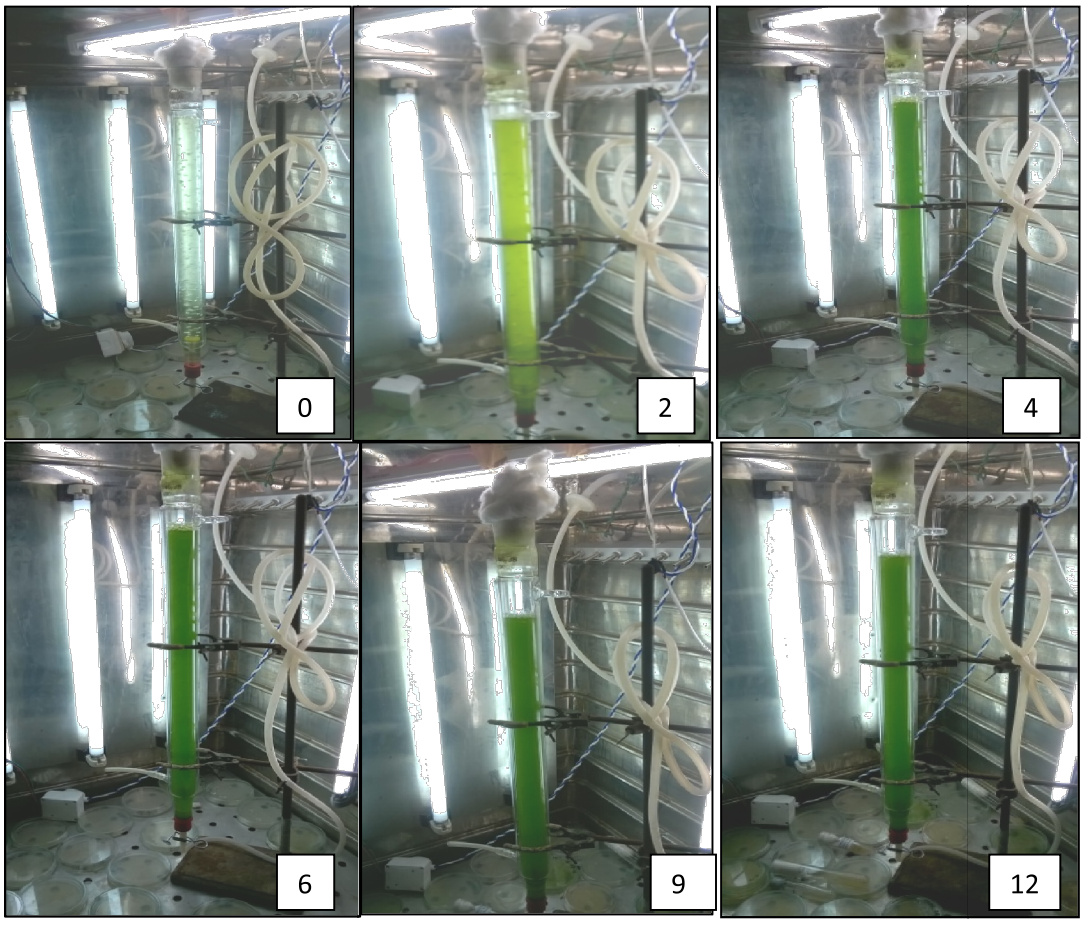

Fig. 4.11: Growth of microalgae in bubble column photobioreactor

Since air contains less than 2% CO_2, therefore the growth of microalgae was higher in the case of 2% CO_2 gas supply.

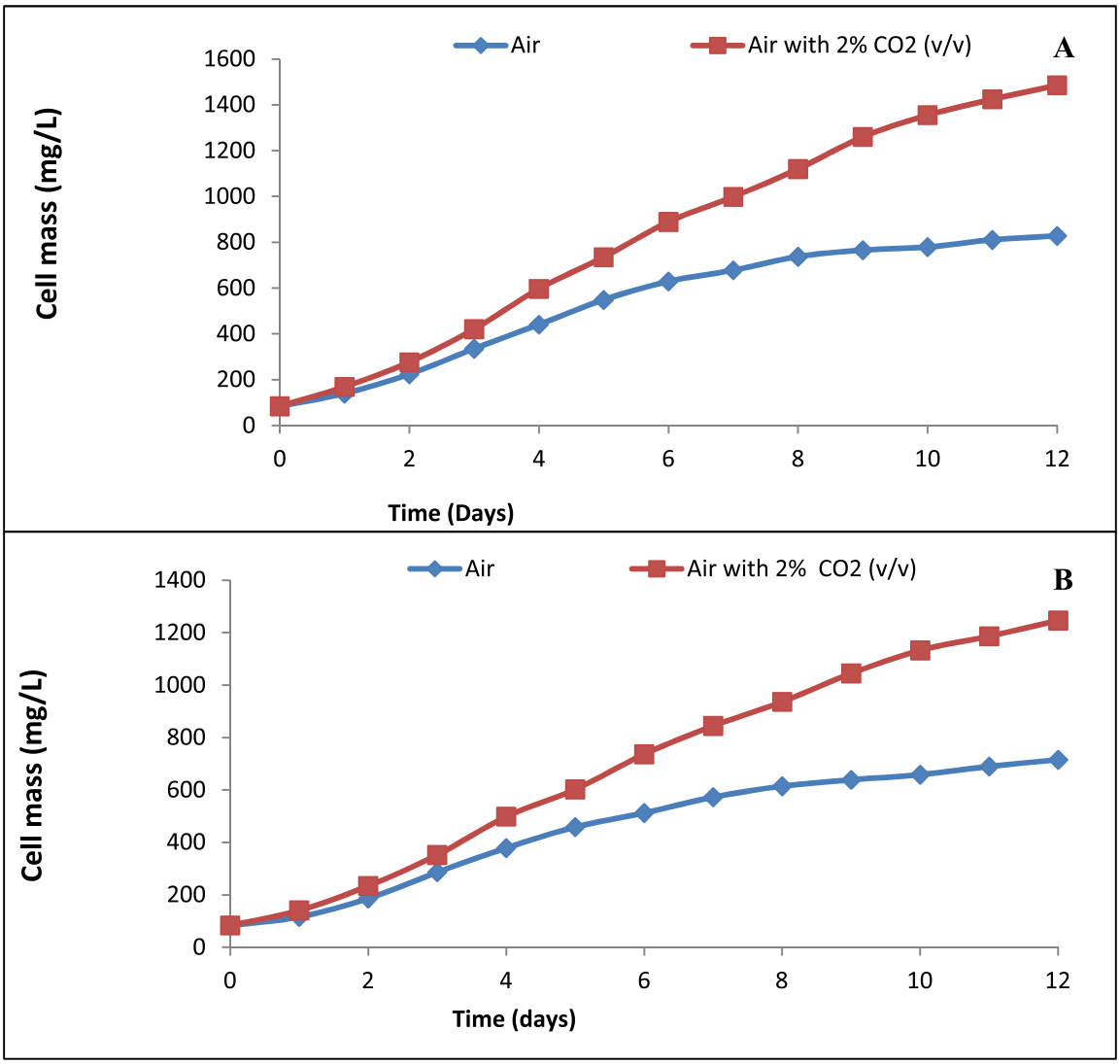

Fig. 4.12: Growth of *C. sorokiniana* (A) and *T. obliquus* (B) in a bubble column reactor

4.2.5.2 Growth study of microalgae in stirred tank photobioreactor (STPBR)

The microalgae were grown in stirred tank photobioreactor for 12 days as shown in Figure 4.13. The growth profile of both microalgae *C. sorokiniana* and *T. obliquus* are shown in Figure 4.14 (a) and figure 4.14 (b) respectively. The specific growth rates of *C. sorokiniana* were found as 0.259 day^{-1} and 0.360 day^{-1} in STPBR with air and 2% CO_2. Similarly, the

specific growth rates of *T. obliquus* were found as 0.227 day^{-1} and 0.317 day^{-1} with air and 2% CO_2. The microalgae biomass productivities of *C. sorokiniana* were obtained as 120.87 mg L^{-1} $day^{-1}$and 59.27 mg L^{-1} day^{-1} with 2% CO_2 and air respectively. The microalgae biomass productivities of *T. obliquus* were obtained as 55.56 mg L^{-1} $day^{-1}$and 102.2 mg L^{-1} $day^{-1}$with air and 2% CO_2 respectively.

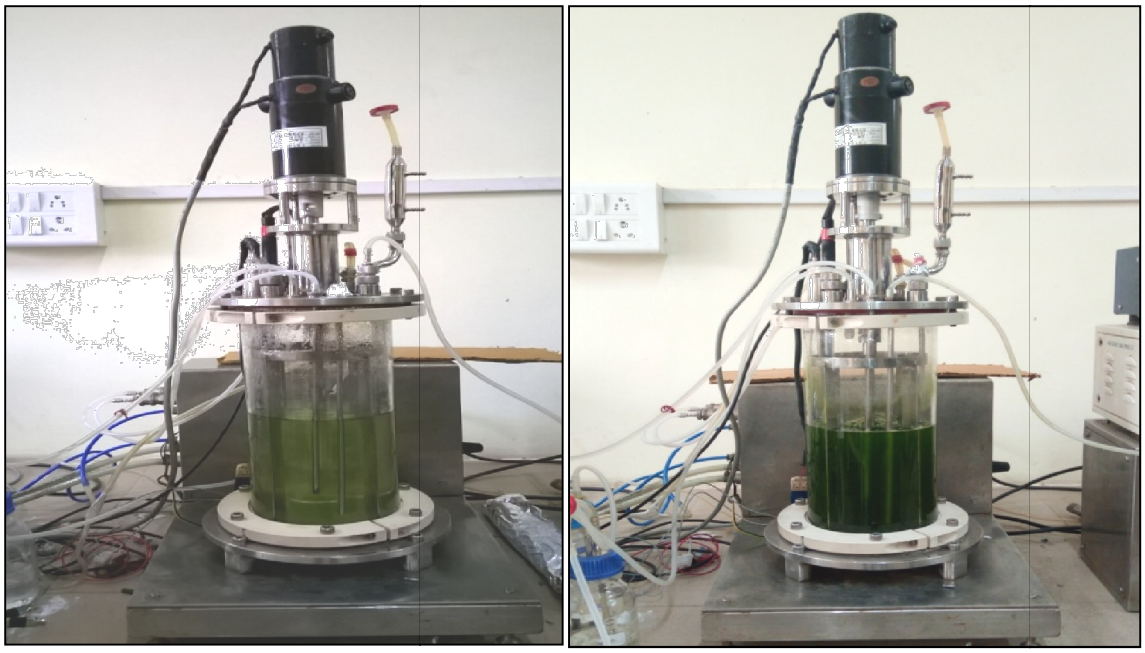

Fig. 4.13: Growth of microalgae at t=0 and t= 12 days

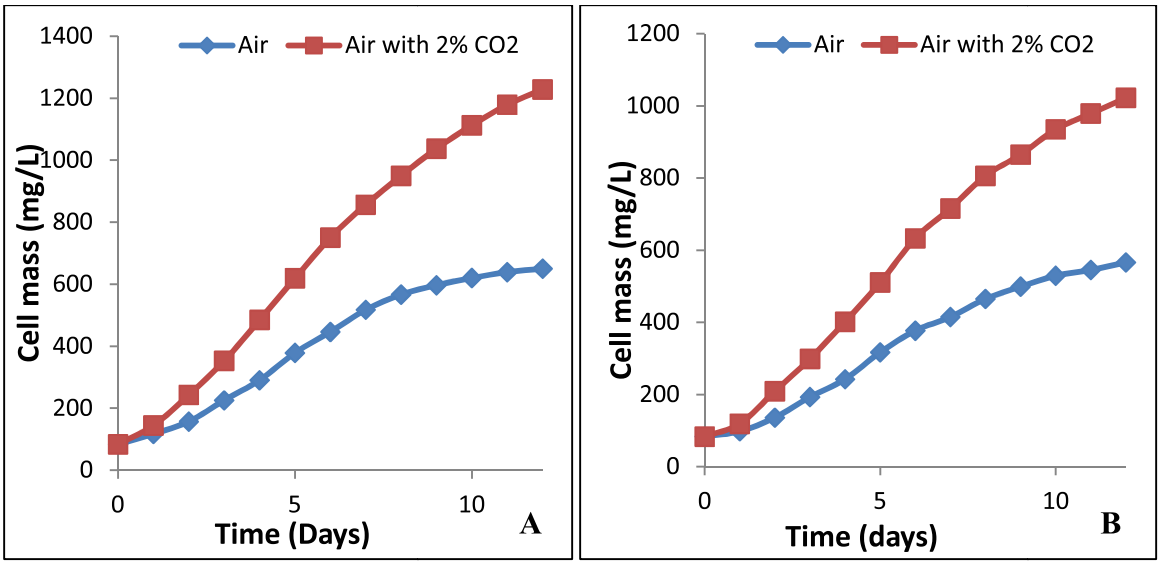

Fig. 4.14: Growth of *C. sorokiniana* (A) and *T. obliquus* (B) in STR

4.2.5.3 Growth study of microalgae in internal loop airlift photobioreactor

The microalgae were grown for 12 days, and the growth of microalgae in the internal loop and external loop airlift photobioreactors is shown in Figure 4.15. After the 12 days of cultivation, the biomass concentration of *C. sorokiniana* with 2 % CO_2 and air reached 1314 mg L^{-1} and 747 mg L^{-1} respectively. The growth of microalgae was compared in both cases i.e. with air and 2% CO_2. However, for the same growth period, *T. obliquus* cell biomass with 2% CO_2 and air reached 1211 mg L^{-1} and 682 mg L^{-1} respectively. The specific growth rate of *C. sorokiniana* with air and 2% CO_2 were achieved as 0.285 day^{-1} and 0.365 day^{-1} respectively. Similarly, the specific growth rate of *T. obliquus* with air and two %CO_2 were found as 0.254 day^{-1} and 0.326 day^{-1} respectively. The growth profiles of microalgae *C. sorokiniana* and *T. obliquus* are shown in Figure 4.16 (a) and 4.16 (b) respectively.

Fig. 4.15: Microalgae growth in the internal loop and external loop air-lift photobioreactor

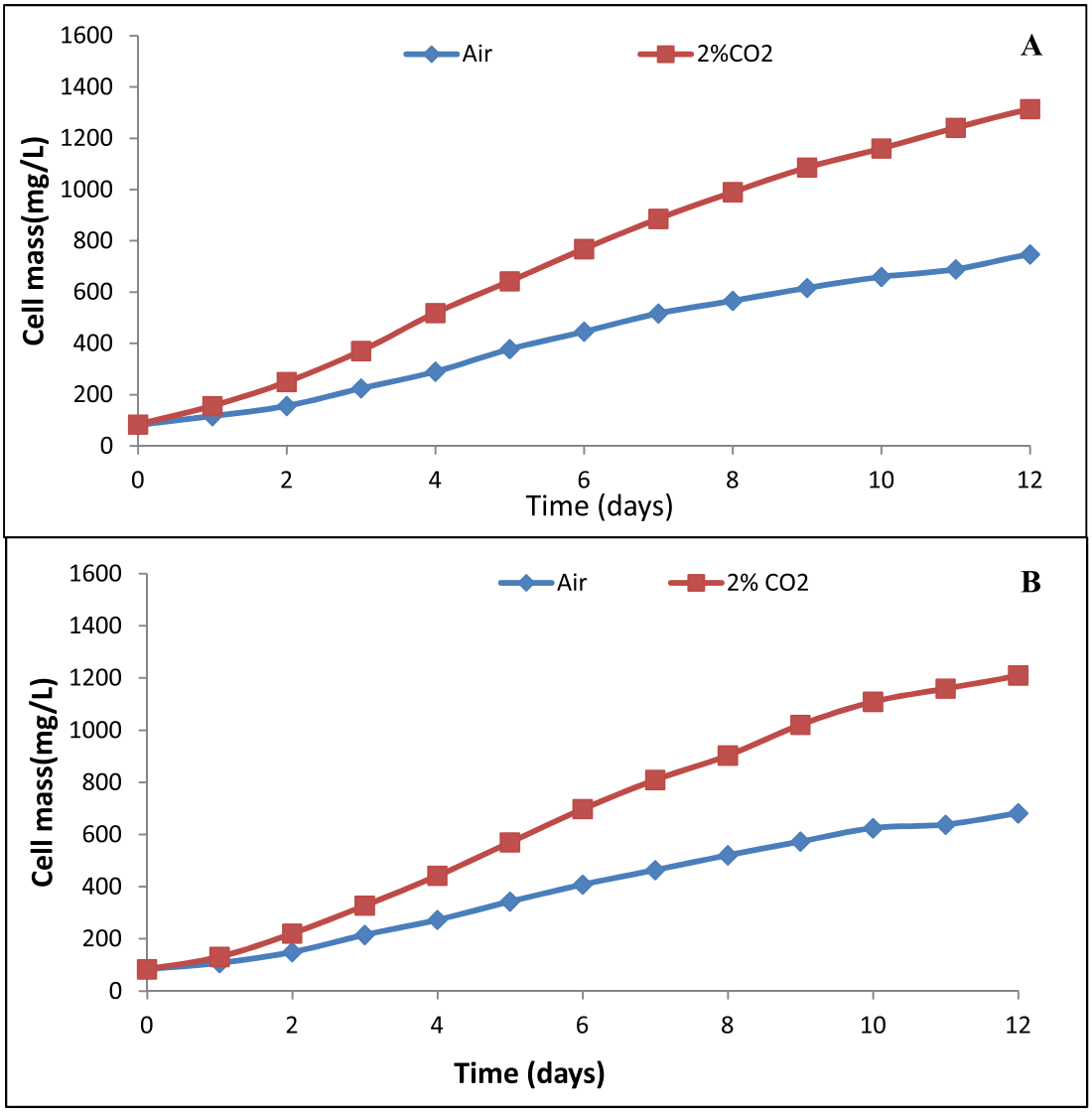

Fig. 4.16: Growth of *C. sorokiniana* (a) and *T. obliquus* (b) in internal loop airlift photobioreactor with air and 2% CO_2

4.2.5.4 Growth study of microalgae in external loop airlift photobioreactor:

The growth profiles of *C. sorokiniana* and *T. obliquus* cultivated in external loop airlift photobioreactor are shown in Figure 4.17 (a) and Figure 4.17 (b). The cell mass concentration of microalgae *C. sorokiniana* reached 1498 mg L^{-1} and 913 mg L^{-1} after 12 days of cultivation with 2% CO_2 and air respectively. The specific growth rates of *C. sorokiniana* were found as 0.342 day^{-1} and 0.392 day^{-1} with air and 2%CO_2 respectively.

Similarly, the biomass concentration of *T. obliquus* reached 1378 mg L^{-1} and 715 mg L^{-1} with 2% CO_2 and air respectively. The specific growth rates of *T. obliquus* were achieved as 0.284 day^{-1} and 0.339 day^{-1} with air and 2% CO_2 respectively. The mean values of specific growth rates of *C. sorokiniana* and *T. obliquus* in different photobioreactors are compared and shown in Figure 4.18 and 4.19 respectively (data significant at $p < 0.05$). The standard deviations of the mean values are shown as error bars. The statistical analysis was performed and p-value <0.05 was obtained.

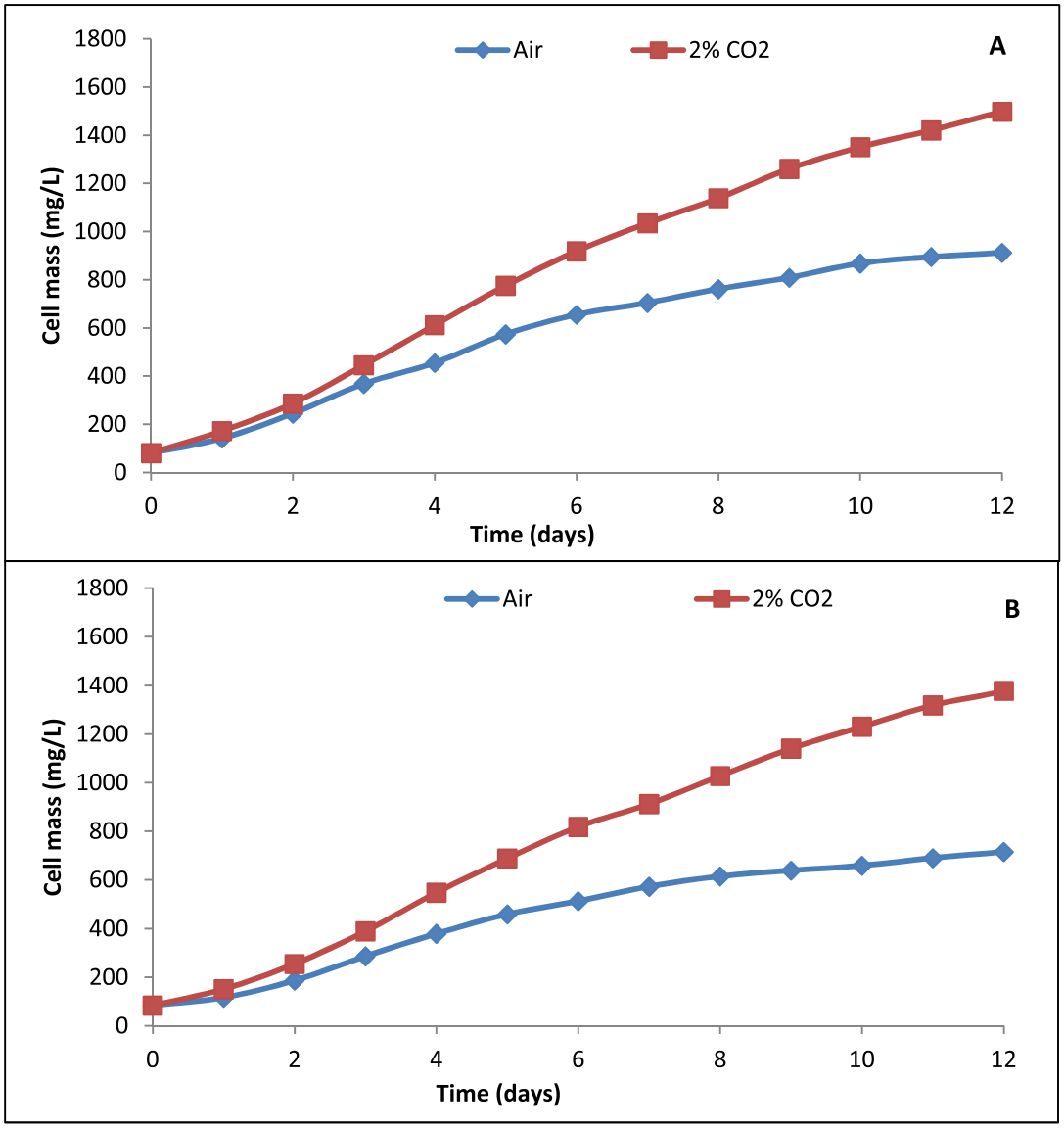

Fig. 4.17: Growth of *C. sorokiniana* (A) and *T. obliquus* (B) in external loop airlift photobioreactor with air and 2% CO_2

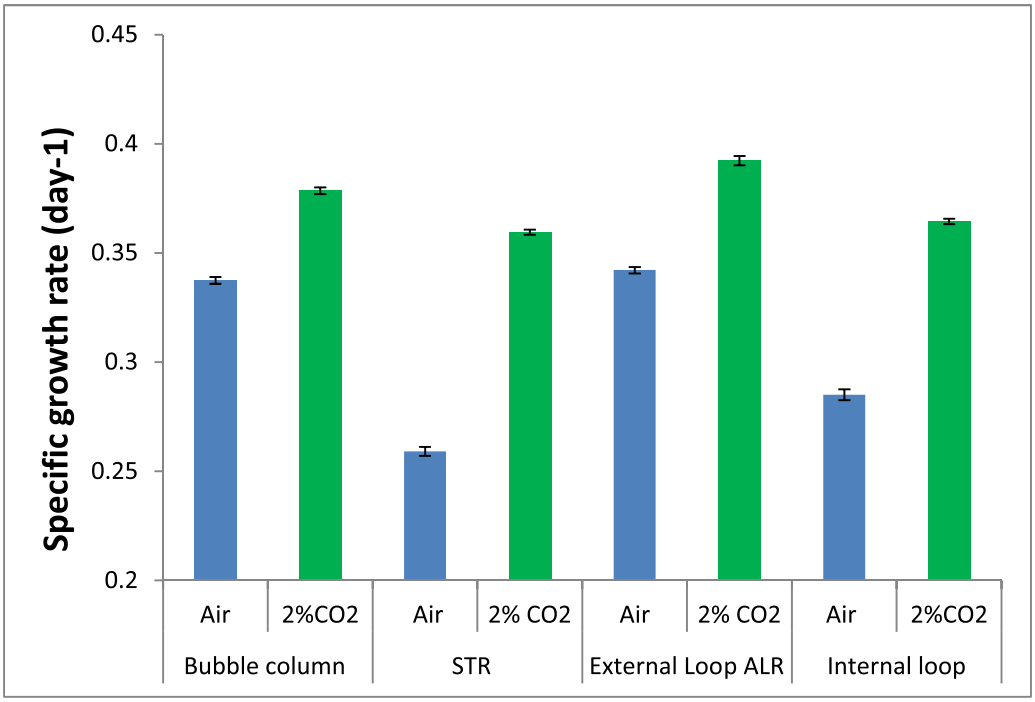

Fig. 4.18: The specific growth rates of *C. sorokiniana* in different photo-bioreactors

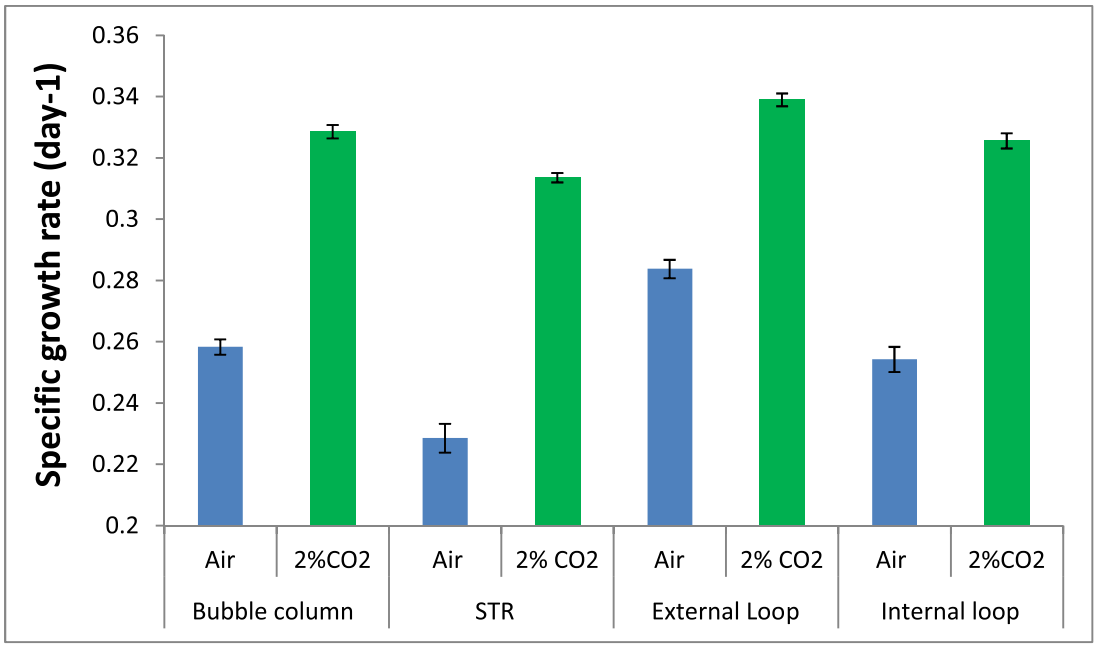

Fig.4.19: Specific growth rates of *T. obliquus* in different photo-bioreactors

4.2.6 Biomass, carbohydrate and starch productivities of *C. sorokiniana* in a bubble column, stirred tank, external loop airlift, and internal loop airlift photobioreactors

The Biomass, carbohydrate and starch productivities of *C. sorokiniana* in a bubble column, stirred tank, external loop airlift, and internal loop airlift photobioreactors were compared and shown in Figure 4.20 (data significant at $p < 0.05$). The standard deviations of the mean values are shown as error bars. The biomass productivities of *C. sorokiniana* were achieved as 135.5 mg L^{-1} day^{-1}, 120.9 mg L^{-1} day^{-1}, 147.8 mg L^{-1} day^{-1} and 126.6 mg L^{-1} day^{-1} with 2% CO_2 aeration in a bubble column, stirred tank, external loop airlift, and internal loop airlift photobioreactors respectively. Whereas with air supply, the biomass productivities of *C. sorokiniana* were obtained as 96.9 mg L^{-1} day^{-1}, 59.3 mg L^{-1} day^{-1}, 100.6 mg L^{-1} day^{-1} and 73.9 mg L^{-1} day^{-1} in a bubble column, stirred tank, external loop airlift, and internal loop airlift photobioreactors respectively. The reason for getting higher biomass productivities in external loop airlift photobioreactor may be the large surface area for illumination and also a whole gas exchange during circulation of the media. Circulation and gas exchange in photobioreactor provide sufficient mass transfer to remove the accumulated O_2 that can inhibit the growth of microalgae, also reduce the algal cells to settle down.

The carbohydrate productivities of *C. sorokiniana* were found as 46.1 mg L^{-1} day^{-1}, 41.1 mg L^{-1} day^{-1}, 43.03 mg L^{-1} day^{-1} and 50.3 mg L^{-1} day^{-1} in a bubble column, stirred tank, internal loop airlift, and external loop airlift photobioreactors with 2% CO_2 aeration. Similarly, The carbohydrate productivities of *C. sorokiniana* were found as 32.9 mg L^{-1} day^{-1}, 20.2 mg L^{-1} day^{-1}, 25.1 mg L^{-1} day^{-1} and 34.1 mg L^{-1} day^{-1} with air in a bubble column, stirred tank, internal loop airlift, and external loop airlift photobioreactors respectively. Among the studied photobioreactors, the highest carbohydrate productivity was found in external loop photobioreactor. The statistical analysis was performed and p-value<0.05 was obtained.

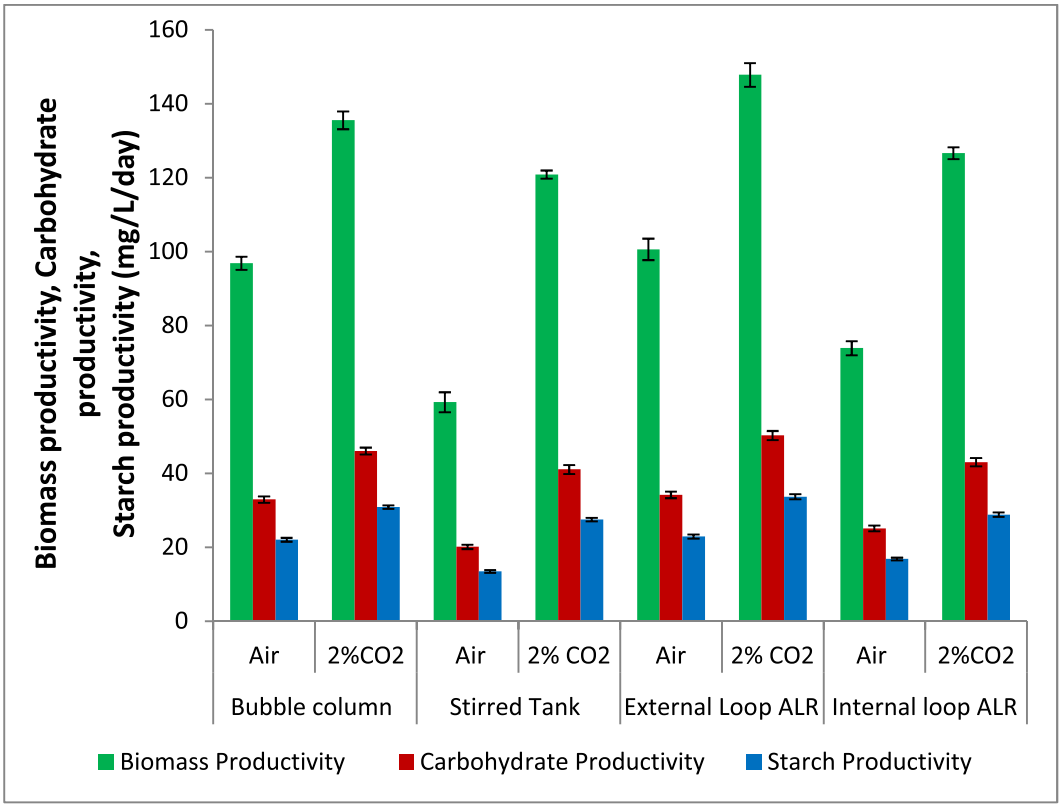

Fig. 4.20: Comparison of biomass, carbohydrate and starch productivities of *C. sorokiniana* bubble column, stirred tank, external loop airlift, and internal loop airlift photo-bioreactors

The starch productivities of *C. sorokiniana* were measured and obtained as 30.9 mg L^{-1} day^{-1}, 27.5 mg L^{-1} day^{-1}, 33.7 mg L^{-1} day^{-1} and 28.9 mg L^{-1} day^{-1} with 2% CO_2 aeration in a bubble column, stirred tank, external loop airlift, and internal loop airlift photobioreactors respectively. Similarly, the starch productivities of *C. sorokiniana* were measured with air and found as 22.1 mg L^{-1} day^{-1}, 13.5 mg L^{-1} day^{-1}, 22.9 mg L^{-1} day^{-1} and 16.8 mg L^{-1} day^{-1} in a bubble column, stirred tank, external loop airlift, and internal loop airlift photobioreactors respectively. The external loop photobioreactors provided the highest biomass, carbohydrate and starch productivities of *C. sorokiniana* with 2% CO_2 aeration.

4.2.7 Biomass, carbohydrate and starch productivities of *T. obliquus* in a bubble column, stirred tank, external loop airlift, and internal loop airlift photobioreactors

The biomass, carbohydrate and starch productivities of *T. obliquus* in a bubble column, stirred tank, external loop airlift, and internal loop airlift photobioreactors were compared and shown in Figure 4.21 (data significant at $p < 0.05$).). The standard deviations of the mean values are shown as error bars. With 2% CO_2 supply, the biomass productivities of *T. obliquus* were achieved as 120.7 mg L^{-1} day^{-1}, 102.2 mg L^{-1} day^{-1}, 130.4 mg L^{-1} day^{-1} and 115.8 mg L^{-1} day^{-1} in a bubble column, stirred tank, external loop airlift, and internal loop airlift photobioreactors respectively. The biomass productivities of *T. obliquus* with air supply were obtained as 69.6 mg L^{-1} day^{-1}, 55.6 mg L^{-1} day^{-1}, 81.8 mg L^{-1} day^{-1} and 66.4 mg L^{-1} day^{-1} respectively. The highest biomass productivity for both the cases with air and 2% CO_2 for aeration were obtained using external loop airlift photobioreactor. The statistical analysis was performed and p-value<0.05 was obtained.

The carbohydrate productivities of *T. obliquus* were found as 47.6 mg L^{-1} day^{-1}, 40.3 mg L^{-1} day^{-1}, 51.4 mg L^{-1} day^{-1} and 45.6 mg L^{-1} day^{-1} in a bubble column, stirred tank, external loop airlift, and internal loop airlift photobioreactors with 2% CO_2 aeration. Similarly, The carbohydrate productivities of *T. obliquus* with air supply were achieved as 27.4 mg L^{-1} day^{-1}, 21.9 mg L^{-1} day^{-1}, 32.2 mg L^{-1} day^{-1} and 26.2 mg L^{-1} day^{-1} in a bubble column, stirred tank, external loop airlift, and internal loop airlift photobioreactors respectively.

The starch productivities of *T. obliquus* were measured and obtained as 31.9 mg L^{-1} day^{-1}, 27.0 mg L^{-1} day^{-1}, 34.4 mg L^{-1} day^{-1} and 30.6 mg L^{-1} day^{-1} with 2% CO_2 aeration in a bubble column, stirred tank, external loop airlift, and internal loop airlift photobioreactors respectively. Similarly, the starch productivities of *T. obliquus* were measured with air and

achieved as 18.4 mg L^{-1} day^{-1}, 14.7 mg L^{-1} day^{-1}, 21.6 mg L^{-1} day^{-1} and 17.5 mg L^{-1} day^{-1} in a bubble column, stirred tank, external loop airlift, and internal loop airlift photobioreactors respectively. The external loop photobioreactors provided the highest biomass, carbohydrate and starch productivities of *T. obliquus* with 2% CO_2 supply.

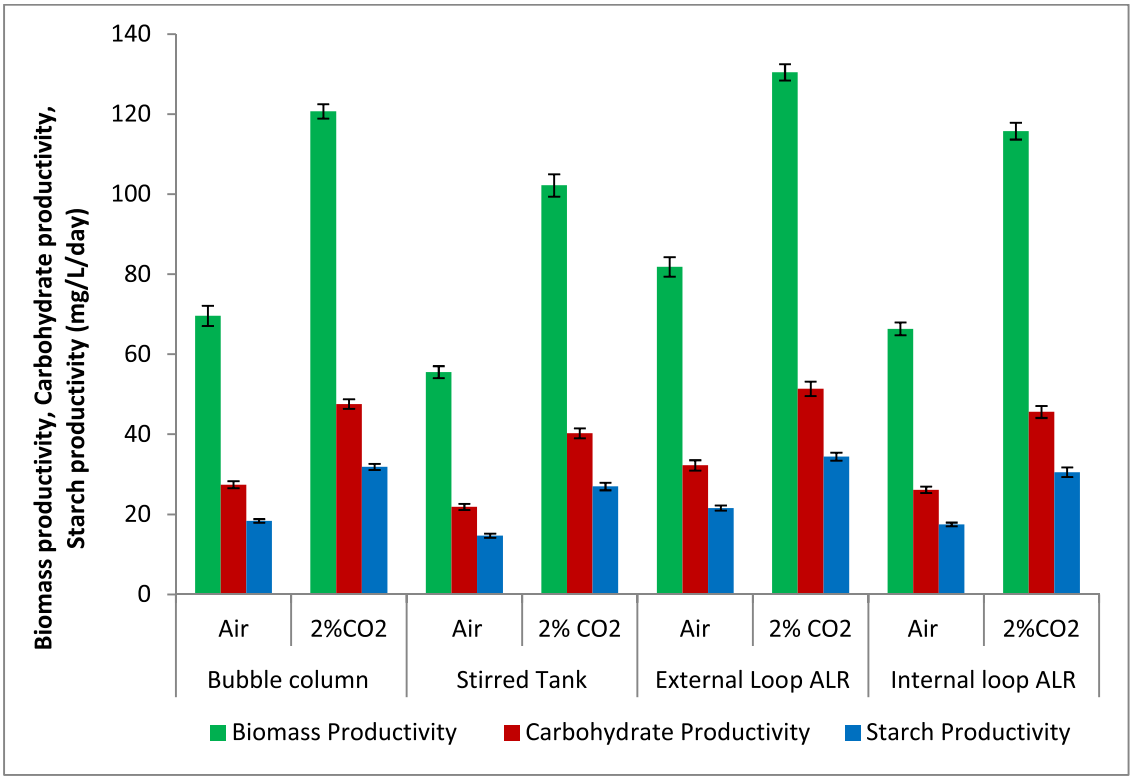

Fig. 4.21: Comparison of biomass, carbohydrate and starch productivities of *T. obliquus* in a bubble column, stirred tank, external loop airlift, and internal loop airlift photo-bioreactors

4.3 Carbohydrate enhancement

The effects of different chemical treatments and nutrient starvation on microalgal carbohydrate, starch and lipid production were studied.

4.3.1 Effect of cycloheximide on carbohydrate, starch and lipid content of microalgae

The antibiotic cycloheximide, a proteosynthesis inhibitor, prevents the nuclear division and cell division in microalgae culture (Zachleder et al., 2002; Brányiková et al., 2011). The

effect of cycloheximide treatment on total carbohydrate, starch and lipid content of *C. sorokiniana* for five days is shown in Figure 4.22. After the addition of cycloheximide during the deceleration phase of the microalgae cell cycle, the total carbohydrate and starch content were increased for two days and further decreased. The carbohydrate content increased from 34 % to 51.7% (w/w) in two days but further, it decreased to 29.4%. Similarly, the starch content was increased to its maximum from 22.5% to 35.2% in two days but later decreased in the next three days to 18.5% (w/w). However, the increase in lipid content of *C. sorokiniana* was less in the first two days, but it significantly increased after two days from 28.1% to 39.5%.

In microalgae, starch is considered as the primary energy storage molecule. However, as the microalgae experience the stress conditions, it accumulates the energy in the form of lipid. Therefore, the decrease in starch content after two days is due to an increase in lipid content (Fernandes et al., 2013). Hence, the microalgae must be harvested after two days of cycloheximide treatment for the production of ethanol. Brányiková et al. (2011) also investigated the effect of cycloheximide on starch content of *Chlorella sp*. and reported that cycloheximide-treated cells accumulated a high starch content (60%,w/w) for up to two days (Brányiková et al., 2011).

Figure 4.23 shows the result of cycloheximide treatment on total carbohydrate, starch and lipid content of *T. obliquus*. The carbohydrate content of *T. obliquus* increased after the cycloheximide treatment from 39.4% to 56.3 % in two days and further it was decreased to 29.8% in the next three days. The starch content of *T. obliquus* was increased to its maximum value from 26.2% to 37.4% within two days after cycloheximide treatment. However, the decreasing profile of starch content was reported after two days and reached 20.5% after the

fifth day of cycloheximide treatment. The lipid content of *T. obliquus* increased slowly and reached its maximum value of 37.1% after the fifth day of treatment.

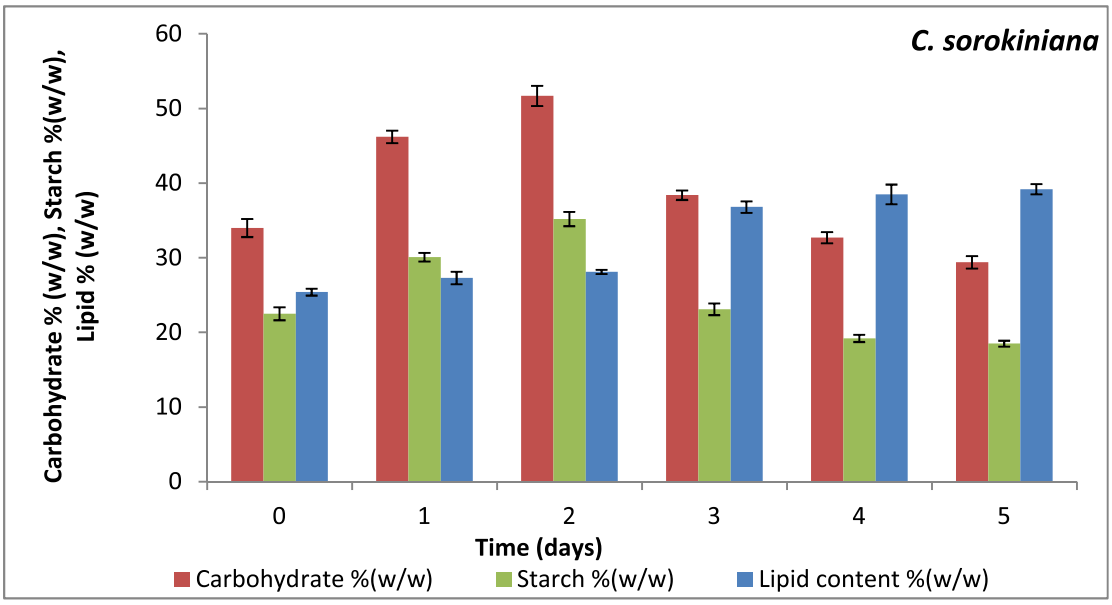

Fig. 4.22: The carbohydrate, starch & lipid content of *C. sorokiniana* after Cycloheximide treatment

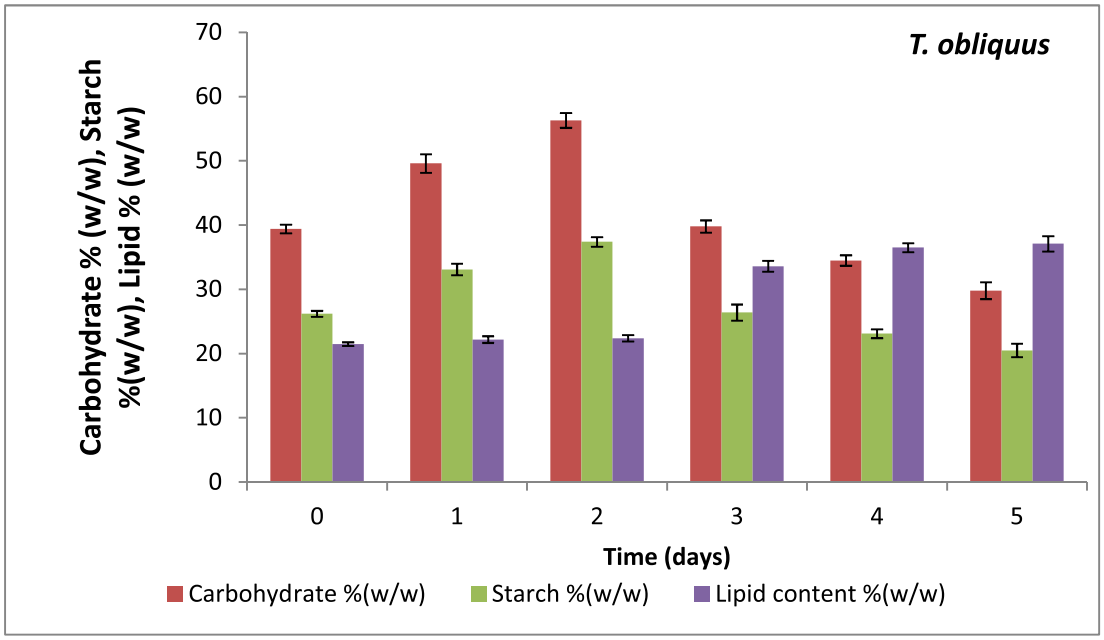

Fig. 4.23: The carbohydrate, starch & lipid content of *T. obliquus* after cycloheximide treatment

4.3.2 Effect of cerulenin on carbohydrate, starch and lipid content of microalgae

A lipid synthesis inhibitor cerulenin binds to β-keto-acyl-ACP synthase. This is component of fatty acid synthase (FAS). The binding blocks the interaction of malonyl-CoA to its enzyme and inhibits fatty acid synthesis. This fatty acid synthesis inhibition causes enhancement of carbohydrate accumulation inside the cells. Both the microalgae were treated with cerulenin, and the results of the treatment were observed. The effect of cerulenin on the carbohydrate, starch and lipid content of *C. sorokiniana* are shown in Figure 4.24. After the five days of treatment, the carbohydrate content of *C. sorokiniana* increased from 34.0% (w/w) to 44.7% (w/w) and starch content increased from 22.5% (w/w) to 29.3% (w/w) respectively. However, the lipid content of *C. sorokiniana* decreased from 25.4% (w/w) to 12.6 % (w/w).

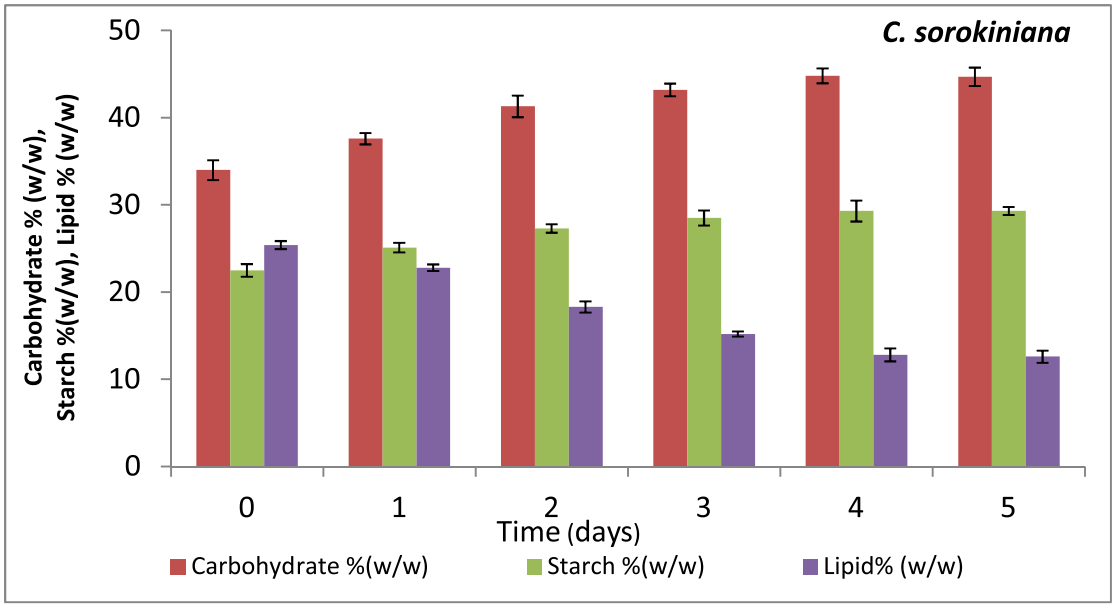

Fig. 4.24: The carbohydrate, starch and lipid content of *C. sorokiniana* after cerulenin treatment

Figure 4.25 shows the result of cerulenin treatment on carbohydrate, starch and lipid content of *T. obliquus* for five days. Cerulenin also inhibited the lipid synthesis in *T. obliquus*. In *T.*

obliquus after cerulenin treatment, the carbohydrate content increased from 39.4% (w/w) to 48.3% (w/w) and the starch content increased from 26.3% (w/w) to 32.3% (w/w). However, the lipid content decreased from 21.5% (w/w) to 10.3% (w/w). The lipid content in *T. obliquus* was lower as compared to the lipid content of *C. sorokiniana.*

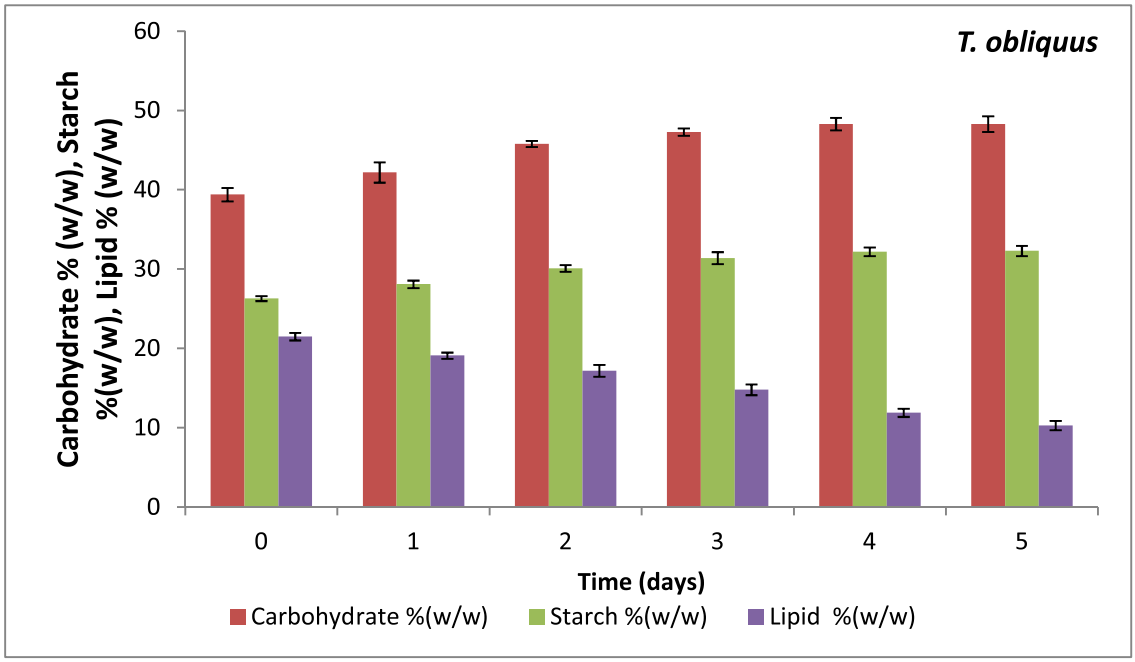

Fig. 4.25: The carbohydrate, starch & lipid content of *T. obliquus* after cerulenin treatment

4.3.3 Enhancement of carbohydrate content using nutrient limitation strategy

Similar to plants, microalgae assimilate the carbon dioxide by photosynthesis in the form of carbohydrate. The carbohydrates are further utilized through several metabolic pathways. The major nutrients required for the growth of microalgae include nitrogen, phosphorus, sulfur, and carbon. The deficiency of nutrients leads to a decrease in growth rate and also changes the cell mass composition (Juneja et al., 2013).

The effect of nitrogen, phosphorus and sulfur limitation on the carbohydrate content of *C. sorokiniana* is shown in Figure 4.26. Under nitrogen, phosphorus and sulfur limiting condition, the carbohydrate content of *C. sorokiniana* was increased from 34% to 54.77%, 39.9% and 46.6% respectively after four days of cultivation. However, if the microalgae were grown further, there was a decrease in carbohydrate content was found and this may be due to carbon flow towards the lipid biosynthesis. The highest carbohydrate content was found in limited nitrogen medium. Ji *et al.* also investigated that nitrogen limitation increased the carbohydrate content by fourfold in *Tetraselmis subcordiformis* (Ji et al., 2011). Ho *et al.* reported a 29% increase in carbohydrate content of *S. obliquus* CNW-N under nitrogen limiting growth condition (Ho et al., 2012). Similarly, Markou *et al.* observed that under phosphorus limiting condition the carbohydrate content of *Arthrospira plantesis* increased from 11 to 67% (Markou and Georgakakis, 2011).

The result of the nutrient limitation on the carbohydrate content of *T. obliquus* is shown in Figure 4.27. The carbohydrate content of *T. obliquus* was increased from 39.4% to 56.7%, 46.9%, and 49.9% after four days of cultivation under nitrogen, phosphorus and sulfur limiting conditions respectively. After reaching the highest carbohydrate content, further growth of microalgae under nutrient limitation led to a decrease in carbohydrate content. The slight decrease in carbohydrate content after four days may be due to the consumption of some of the carbohydrates for other metabolic activities. In this study, the most substantial amount of carbohydrates was accumulated in both microalgae under nitrogen deprived conditions.

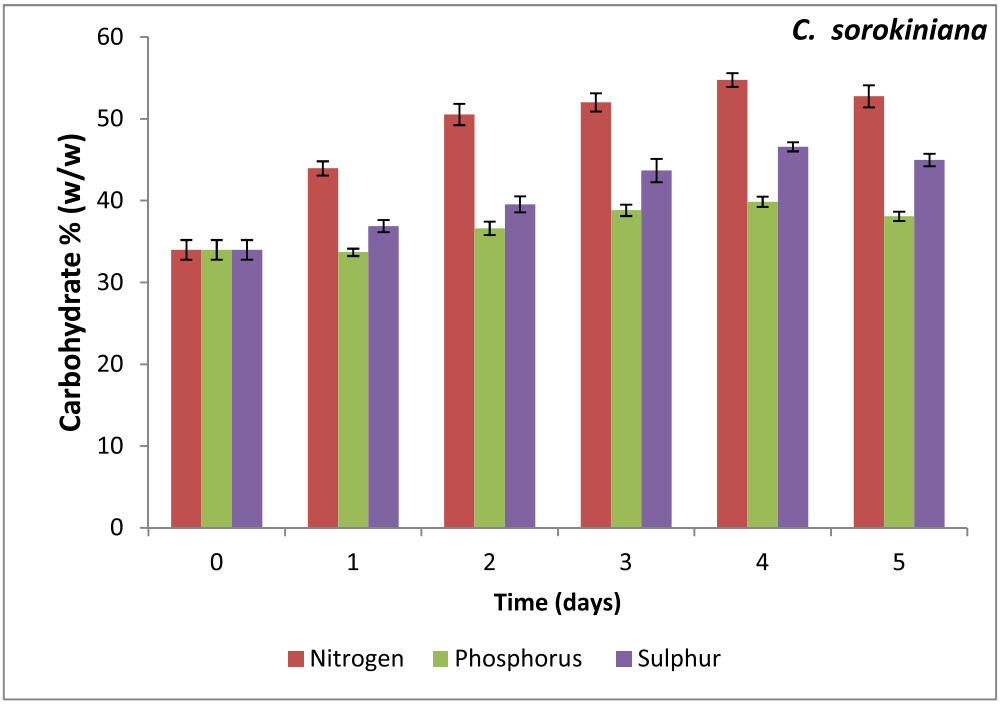

Fig. 4.26: The carbohydrate content of *C. sorokiniana* after nitrogen, phosphorus and sulphur limitation

4.3.4 Microalgae starch content after the nutrient limitation

The effect of nutrient limitation on the starch content of *C. sorokiniana* is shown in Figure 4.28. The starch content of *C. sorokiniana* was increased from 22.8% to 36.7%, 26.7% and 31.2% after four days of cultivation under nitrogen, phosphorus and sulfur limitation conditions respectively. The nitrogen starvation affected the protein synthesis, and the increase in starch content is due to diversion of carbon flow from protein to starch synthesis under nitrogen limitation growth. Similar results were found with other studies. Korean et al. investigated the effect of nitrogen depletion on the growth and carbohydrate content of *Chlamydomonas maxicana*. Under the nitrogen, depletion growth was ceased. However, the polysaccharide content was increased (Kroen and Rayburn, 1984).

The effect of nutrient limitation on the starch content of *T. obliquus* is shown in Figure 4.29. The carbohydrate contents of *T. obliquus* after four days of cultivation under the nutrient limitation of nitrogen, phosphorus and sulfur increased from 26% to 37.5%, 30.9% and 31.8% respectively.

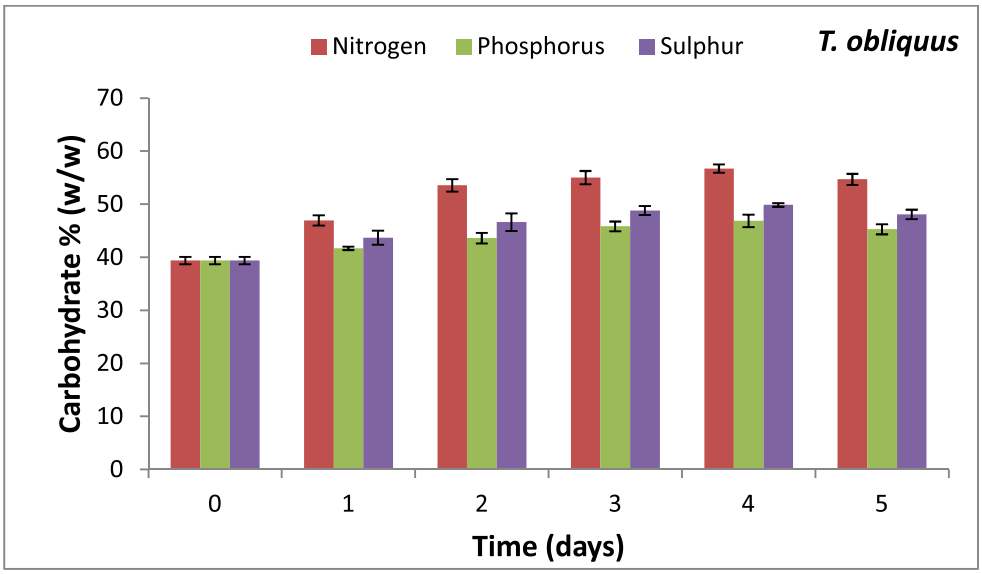

Fig. 4.27: The carbohydrate content of *T. obliquus* after nitrogen, phosphorus and sulphur limitation

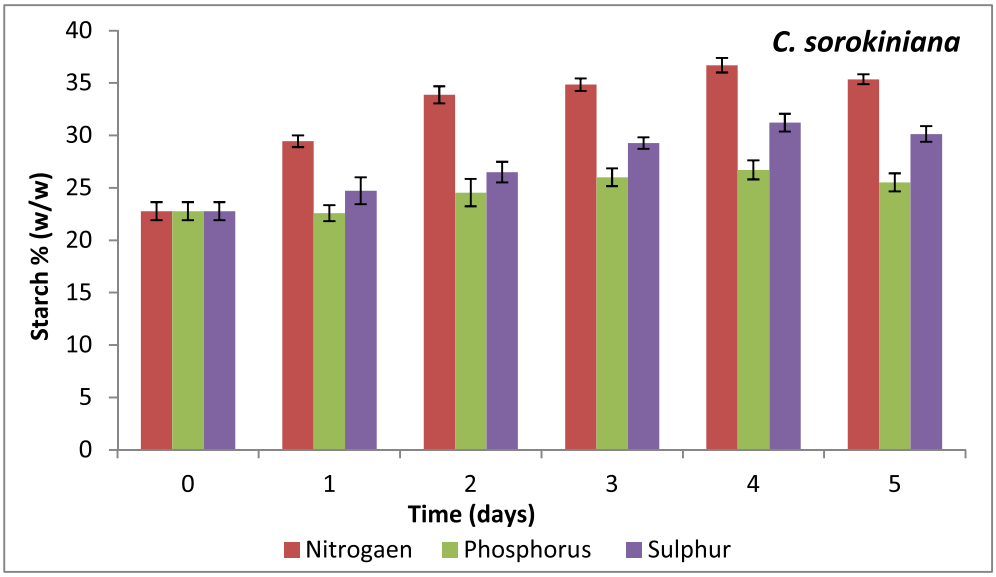

Fig. 4.28: The starch content of *C. sorokiniana* after nitrogen, phosphorus and sulphur limitation

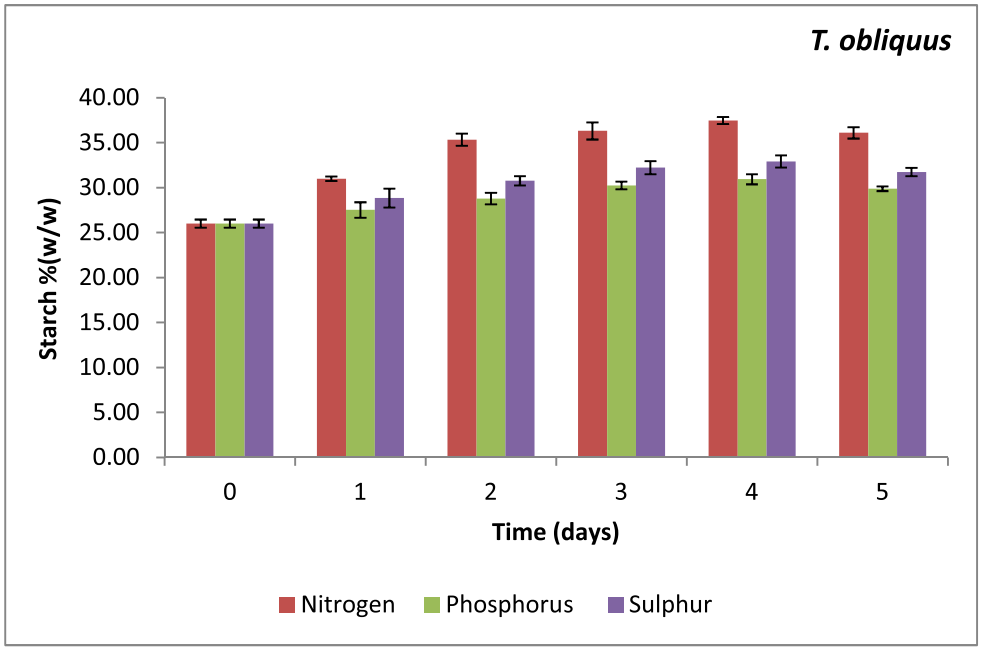

Fig. 4.29: The starch content of *T. obliquus* after nitrogen, phosphorus and sulphur limitation

4.3.5 CHNS analysis of microalgae after nutrient limitation study

Table 4.2 shows the carbon (C), hydrogen (H), nitrogen (N) and sulfur (S) content of *C. sorokiniana* and *T. obliquus* under nutrient-rich and nutrient limiting conditions. Nutrient-rich medium was used for the control experiment. *C. sorokiniana* was grown in nutrient-rich medium and the carbon, hydrogen, and nitrogen contents were found as 40.476%, 5.715% and 6.626% respectively. Under nitrogen limitation, carbon and hydrogen contents of *C. sorokiniana* increased to 41.808%, and 6.356% respectively. However, nitrogen content was decreased from 6.626% to 4.597%. Sulfur content was only detected in *C. sorokiniana* under limited nitrogen growth. The carbon and hydrogen contents of *C. sorokiniana* also increased to 40.948% and 6.029% respectively, and nitrogen content decreased to 5.427% under phosphorus (P) deprived media. Under sulfur-deprived media, *C. sorokiniana* assimilated 41.047% of carbon and 6.192% of hydrogen which were higher than average growth under

sulfur-rich medium. However, the nitrogen content of *C. sorokiniana* under sulfur-deprived was lower than average growth.

Since, nitrogen, phosphorus and sulfur are essential elements of protein and therefore growth under the limitation of these elements led to a reduction in protein synthesis and carbon flows towards more carbohydrate synthesis. The increase in the carbon content confirmed the increase in carbohydrate content because carbon percentage is directly related to the carbohydrate content.

Table 4.2: Carbon, hydrogen, nitrogen, sulfur composition of microalgae biomass

S.N.	Sample name	Sample weight (mg)	N %	C%	H %	S%
1	*Chlorella sorokiniana* growth in nutrient rich media	0.545	6.626	40.476	5.715	n.d.*
2	*C. sorokiniana* growth in N deficient	0.929	4.597	41.808	6.356	1.013
3	*C. sorokiniana* growth in P deficient media	0.667	5.427	40.948	6.029	n.d.
4	*C. sorokiniana* growth in S deficient media	0.738	5.049	41.047	6.192	n.d.
5	*Tetradesmus obliquus* growth in nutrient rich media	2.166	4.784	43.747	6.948	n.d.
6	*T. obliquus* growth in N deficient media	1.984	4.189	45.984	7.438	n.d.
7	*T. obliquus* growth in P deficient media	1.998	4.698	44.198	7.262	n.d.
8	*T. obliquus* growth in S deficient media	2.184	4.384	44.748	7.289	n.d.

* n.d. - not detected

The microalgae, *T. obliquus*, were grown in nutrient-rich media and its carbon, hydrogen, and nitrogen contents were found as 43.747%, 6.948% and 4.784% respectively. Under the nitrogen deprived growth condition, the carbon and hydrogen contents of *T. obliquus* increased and found to be 45.984% and 7.438% respectively. However, the nitrogen content of *T. obliquus* decreased and was found to be 4.189%. The carbon and hydrogen contents of *T. obliquus* in phosphorus deprived media also increased and found as 44.198% and 7.262% respectively. However, the nitrogen content of *T. obliquus* decreased to 4.698% under phosphorus limiting growth condition. *T. obliquus* assimilated 44.748% of carbon, 7.289% of hydrogen and 4.384% of nitrogen under sulfur-deprived condition. The highest carbon content of *T. obliquus* was found in case of nitrogen limiting growth, and therefore these results confirmed that highest carbohydrate content was obtained with nitrogen deprived media for both microalgae.

4.4 Extraction of carbohydrate (starch) using different pre-treatment method

Microalgae polysaccharides are encapsulated in the cell wall, which must be released from the cell wall and hydrolysed into simple sugars so that microorganisms (yeast/bacteria) can ferment it to bioethanol. Pretreatment of microalgae is usually a costly step in bioethanol production; thus, an economical pretreatment method should be applied. An effective pretreatment should be cost-effective, energy efficient, simple to apply, and should not convert the fermentable sugars into an unusable form. Four different pretreatment methods, i.e. acidic (H_2SO_4), alkali (NaOH), ultrasonication, and free radical aided were used and compared for the pretreatment of microalgae, *C. sorokiniana* and *T. obliquus*. The performance of each pretreatment method was determined by measuring the weight (g) of

sugar released per unit weight (g) of total carbohydrate in dry weight of biomass. Figure 4.30 shows the microscopic view of microalgae before and after the pretreatments.

Microalgae → / Pretreatment ↓	*Chlorella sorokiniana*	*Tetradesmus obliquus* IIT BHU BC01
Control	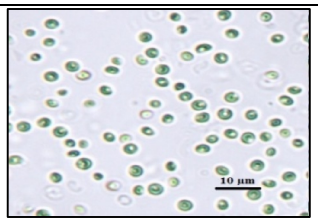	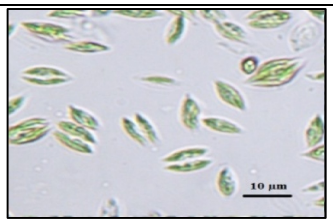
H_2SO_4 (1 N)	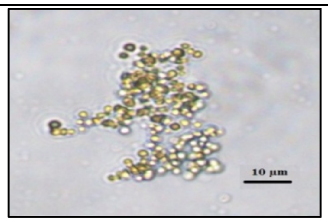	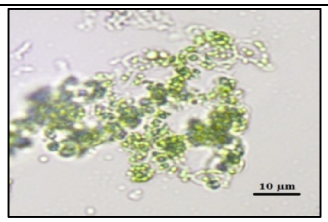
NaOH (1 N)	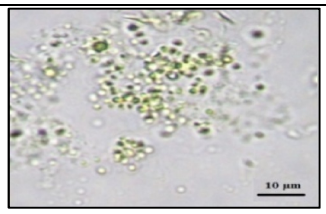	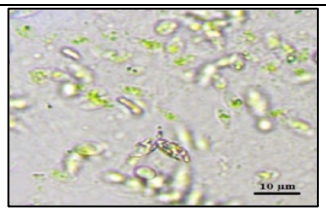
H_2O_2+$FeSO_4$	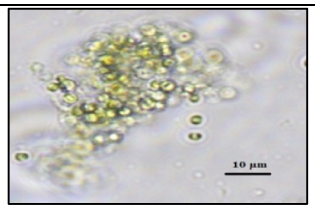	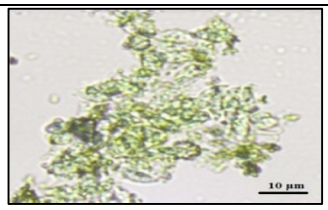
Ultrasonication	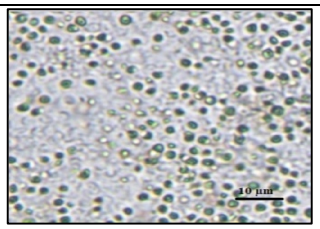	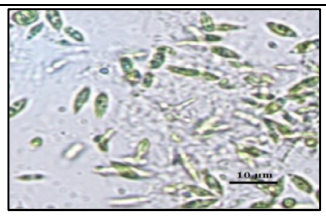
Ultrasonication + Enzymes	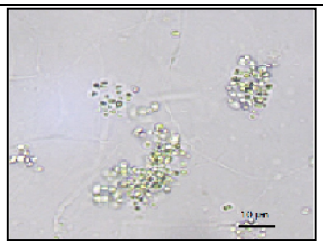	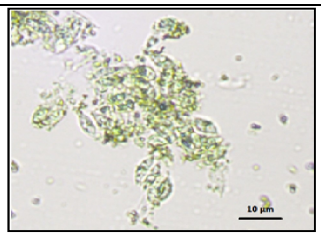

Fig. 4.30: Microscopic view of microalgae before and after the pretreatments

4.4.1 Acidic pretreatment of microalgae

Acid pretreatment enhances the degeneration of the cellulose matrix of the microalgae cell wall. It also causes depolymerisation of hemicelluloses as well as hydrolysis of carbohydrates. Acid pretreatment of microalgae biomass was performed to investigate the effect of different concentration of sulfuric acid (0.25 to 3N) on sugar release. Figure 4.31 shows the effect of different concentration of sulfuric acid on sugar released per gram of microalgae. With the 0.25N concentration of H_2SO_4, the released sugar concentrations were found as 42.5% (w/w) and 49.0% (w/w) for *C. sorokiniana* and *T. obliquus* respectively. As the concentration of sulfuric acid was increased, the released sugars concentration was also increased. The highest free sugar was obtained with 1N of H_2SO_4 concentration in both the microalgae. The released sugar concentration with 1N H_2SO_4 was obtained as 49.0 and 54.8% (w/w) for *C. sorokiniana* and *T. obliquus* respectively. The highest extraction efficiencies with H_2SO_4 were calculated as 89.6 and 96.5% for *C. sorokiniana* and *T. obliquus* respectively. Further increase in acid concentration (above 1N) led to a reduction in total sugar because at high acid concentration some of the sugars are denatured and form furfural or hydroxyl methyl furfural. At an acid concentration of 3N, the released sugar concentration was reduced and reached to 39.3 and 45.4% (g of sugar per g of microalgae) for *C. sorokiniana* and *T. obliquus* respectively. Other researchers also observed similar results of acid pretreatments of microalgae. Nguyen *et al.* investigated the hydrothermal acid pretreatment of *Chlamydomonas reinhardtii* UTEX 90, and they found that maximum sugar release 58% (w/w) was obtained with 3% of sulfuric acid at 110^{o}C for 30 min (Nguyen et al., 2009). Miranda et al. reported that the highest sugar extraction efficiency (95.6%) was

achieved from *Scenedesmus obliquus* by using H_2SO_4 (2N) at 120°C for 30min (Miranda et al., 2012).

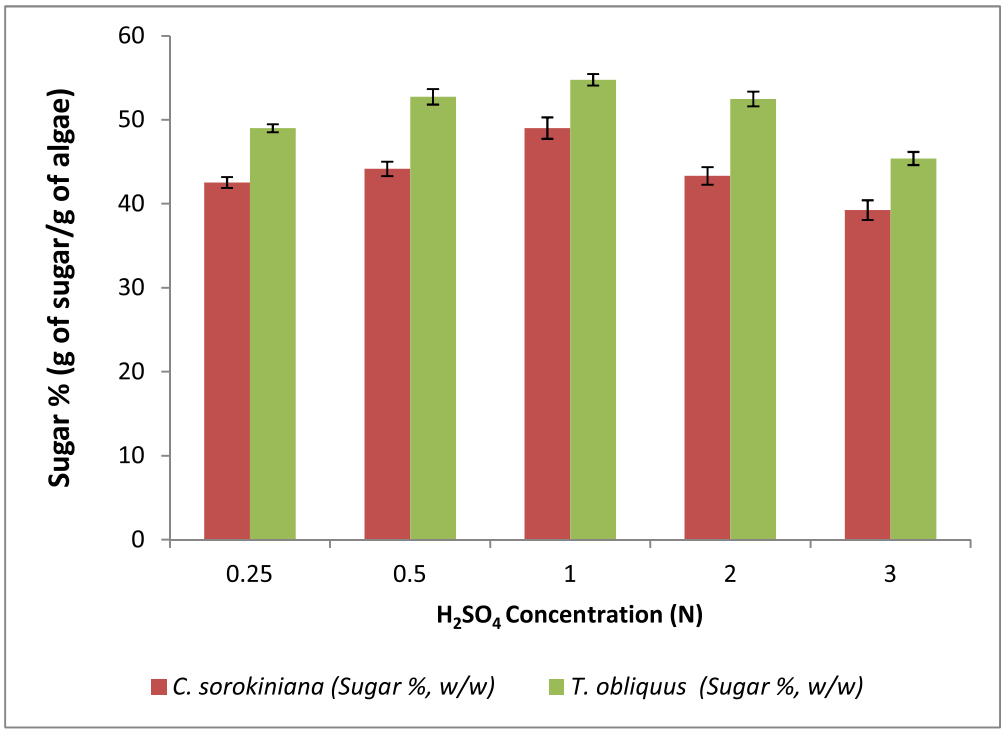

Fig. 4.31: The sugar released after acidic pretreatment of *C. sorokiniana* and *T. obliquus* biomass

4.4.2 Alkali pretreatment of microalgae:-

The alkaline hydrolysis is characterised by saponification of intermolecular ester bonds and creating salvation. Alkaline pretreatment of both the microalgae, *C. sorokiniana* and *T. obliquus,* was performed and the results are shown in Figure 4.32. The microalgae were pretreated with different concentrations (0.5 to 5.0%) of NaOH, and released sugars were estimated to measure the pretreatment efficiency. It was observed from the study that as the concentration of NaOH was increased from 0.5 to 4% (w/w), the released sugars concentration was also increased. However, the concentration of released sugars was not

significantly changed above 4% of NaOH. The highest released sugar concentrations were found as 21.1% (g of sugar /g of microalgae) and 22.5% (g of sugar /g of microalgae) for *C. sorokiniana* and *T. obliquus* respectively, which were achieved with 4% of NaOH. Harun *et al.* also investigated the alkaline pretreatment of *Chloroccum sp.* using 0.75% NaOH at 120°C for 30 min. They determined the highest sugar release after the cell rupturing as 350 mg of sugar per g of microalgae (Harun et al., 2011).

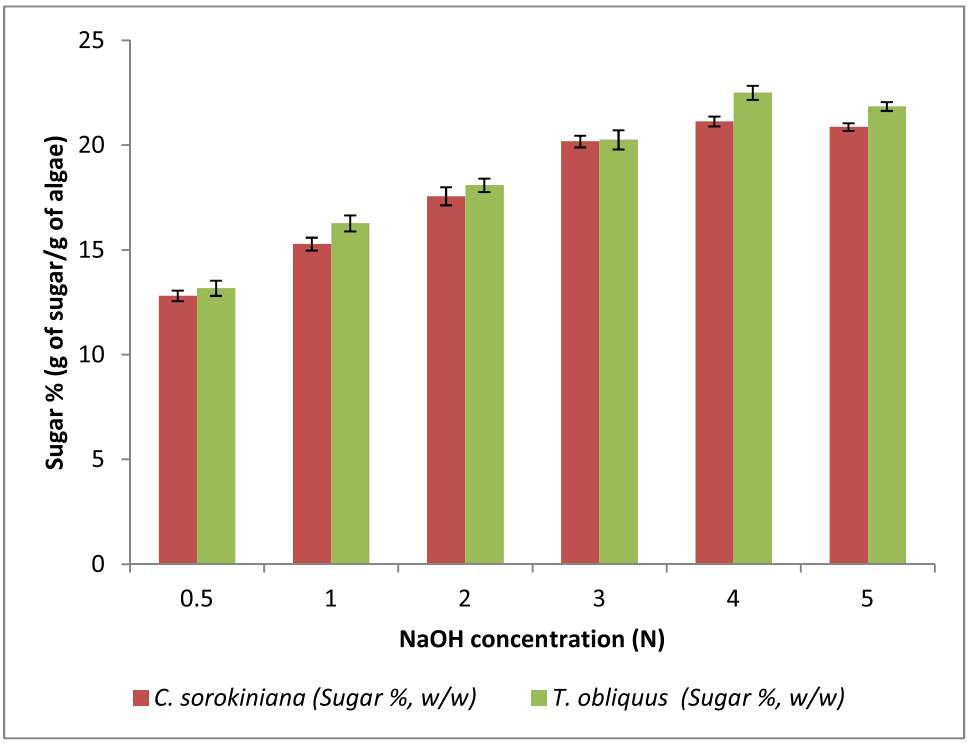

Fig. 4.32: The sugar released after NaOH pretreatment of *C. sorokiniana* and *T. obliquus* biomass

4.4.3 Hydroxyl radical-aided thermal pretreatment

The effects of different concentrations of hydrogen peroxide during hydroxyl aided thermal pretreatment on sugar yield of microalgae biomass of *C. sorokiniana* and *T. obliquus* are

shown in Figure 4.33. The increase in H_2O_2 concentration from 0.06 g/L to 0.18 g/L resulted in an increase in sugar release from 13.3% (w/w) to 15.8 % (w/w) and 13.8 to17.7% (w/w) for *C. sorokiniana* and *T. obliquus* respectively. Further increase in H_2O_2 concentration does not cause any significant difference in sugar release concentrations. Therefore, the 0.18 g/L of H_2O_2 was found as optimum concentration value for sugar release in both *C. sorokiniana* and *T. obliquus.* Gao *et al.*, 2015 also studied the hydroxyl radical-aided thermal pretreatment of microalgae and macroalgae biomass (Gao et al., 2015). They reported that complete (100%) carbohydrate recoveries from microalgae biomass could be achieved using the optimum conditions (100^{o}C, 30min and 5.3 mM H_2O_2). However, in this study 28.8 and 31.2 g/100g of dissolved carbohydrate were extracted using hydroxyl radical-aided thermal pretreatment from *C. sorokiniana* and *T. obliquus* respectively.

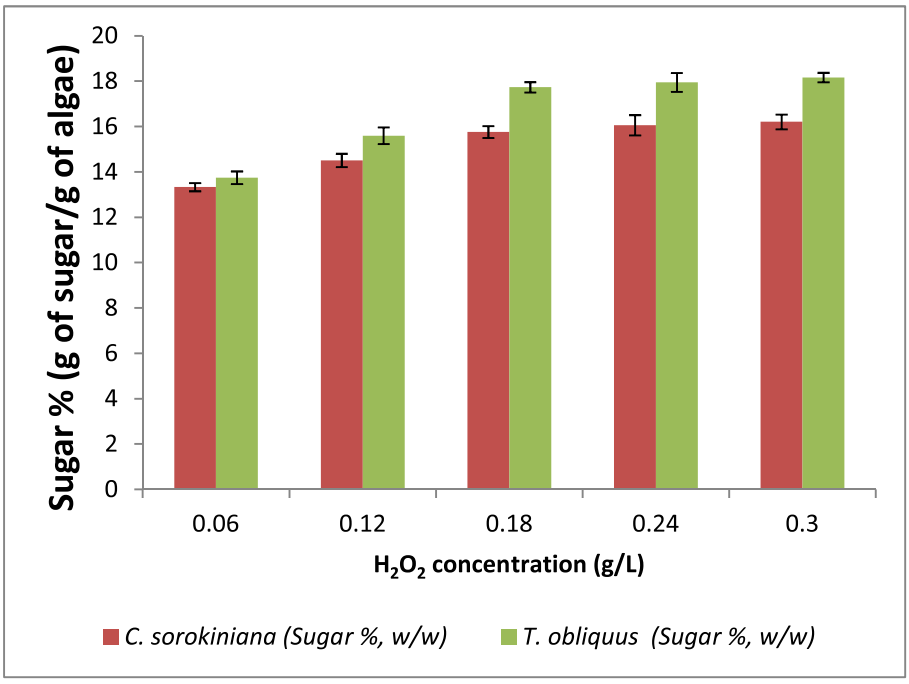

Fig. 4.33: The sugar released after hydroxyl radical-aided thermal pretreatment of *C. sorokiniana* and *T. obliquus* biomass

4.4.4 Ultrasonication pretreatment

The ultrasonication pretreatment of microalgae was performed, and the results are shown in Figure 4.34. This study showed that the increase in sonication time significantly increased the sugar release yield up to 60 min sonication. However, a further increase in sonication time did not show any significant change. The sugar yields with 10 min of sonication time were 2.15 and 5.42 g/100g DCW for *C. sorokiniana* and *T. obliquus* respectively. The sugar yields increased with 60 min of sonication and reached to 14.0 and 15.7 g/100g DCW for *C. sorokiniana* and *T. obliquus* respectively. The extraction efficiency of ultrasonication was found as 25.5 and 27.6 g/ 100g of carbohydrate for *C. sorokiniana* and *T. obliquus* respectively.

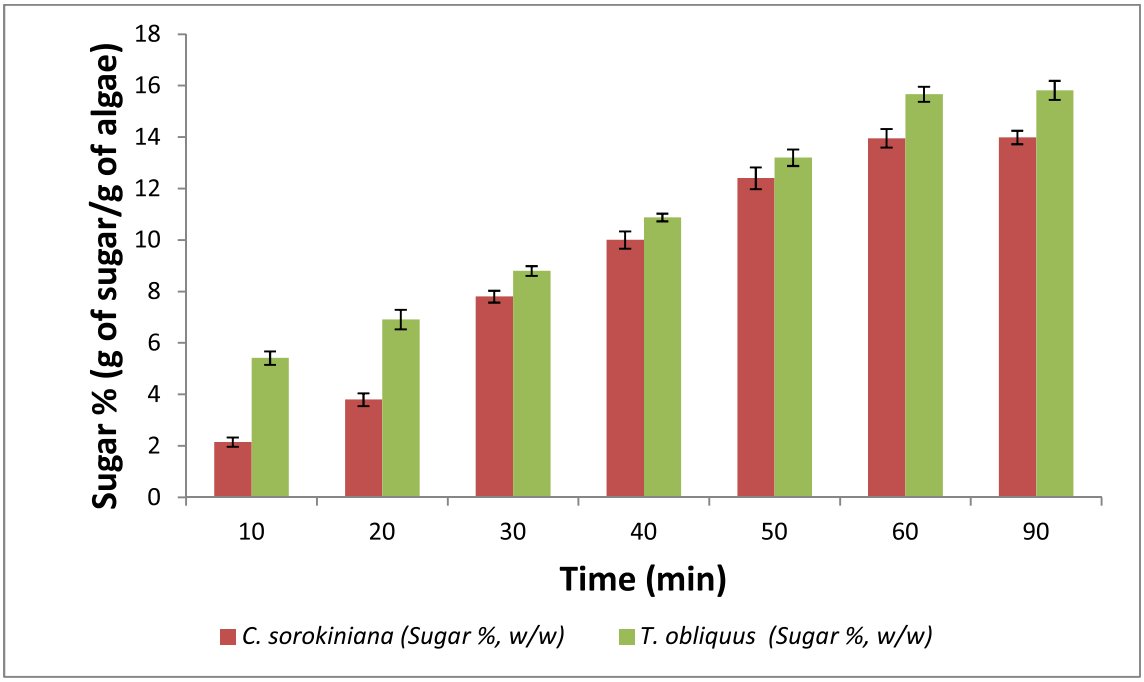

Fig. 4.34: The sugar released after ultrasonication pretreatment of *C. sorokiniana* and *T. obliquus* biomass

4.4.5 Ultrasonication followed by enzymatic pretreatment (UFEP)

Since enzymatic (amylases) treatment alone couldn't be more effective, therefore a mechanical disruption i.e. ultrasonication was coupled with enzymatic pretreatment. It was found that UFEP method improved the pretreatment efficiency because of the combination of α- amylase, amyloglucosidase and cellulase help in liquefaction and saccharification of algal carbohydrate after the cell wall rupture. The effect of enzymatic pretreatment after the ultrasonication is shown in Figure 4.35. After the enzymatic pretreatment, the sugars released were found as 35.4 and 38.9% (g of sugar per g of algae) from *C. sorokiniana* and *T. obliquus* respectively. After combining the ultrasonication and enzymatic pretreatment, the sugar released was increased and reached to 49.9 and 55.3% (g of sugar per g of algae) from *C. sorokiniana* and *T. obliquus* respectively. The extraction efficiencies of combined ultrasonication and enzymatic pretreatment method were calculated as 91.3% and 97.4% for *C. sorokiniana* and *T. obliquus* respectively.

4.4.6 Comparison of pretreatment methods

The extraction efficiencies of different pretreatment methods are shown in Figure 4.36. The highest sugar release was obtained with UFEP method among the other pretreatment methods. The UFEP method provided 91.3% and 97.4% (g of dissolved carbohydrate per g of total carbohydrate) from *C. sorokiniana* and *T. obliquus* respectively. The 1 N sulfuric acid pretreatment provided 89.6% and 96.5% (g of sugar per g of total carbohydrate) from *C. sorokiniana* and *T. obliquus* respectively. The lowest dissolved carbohydrate was obtained with ultrasonication treatment which provided 25.5 and 27.6% (w/w) from *C. sorokiniana* and *T. obliquus* respectively. The alkali pretreatment with 4N of NaOH provided 38.6% and 39.7% (w/w) from *C. sorokiniana* and *T. obliquus* respectively. The hydroxyl radical aided

pretreatment with 0.18g/L of H_2O_2 provided 28.8% and 31.2% (g of sugar per g of total carbohydrate) from *C. sorokiniana* and *T. obliquus* respectively.

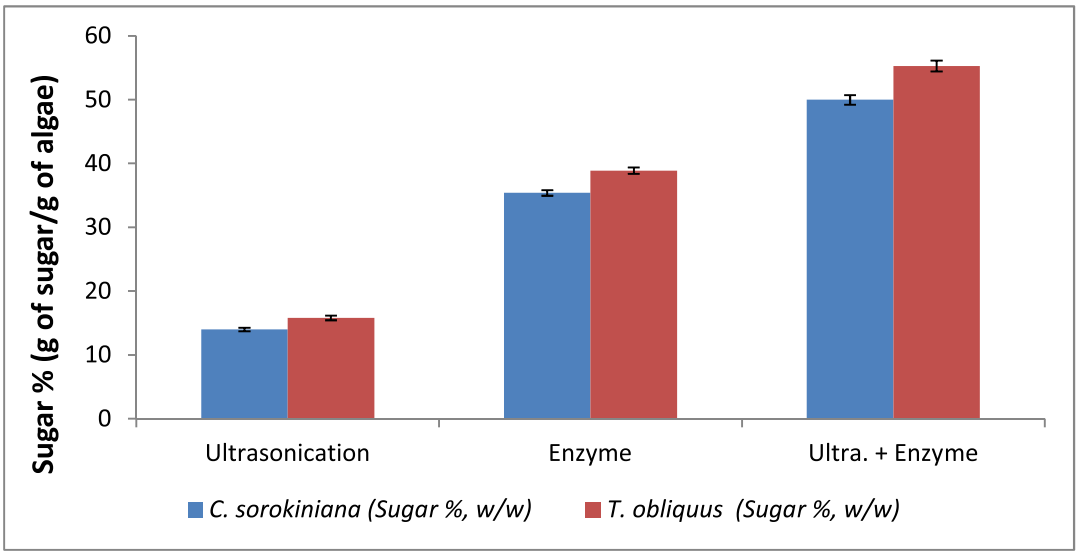

Fig. 4.35: The sugar released after enzymatic pretreatment and ultrasonication followed by enzymatic pretreatment of *C. sorokiniana* and *T. obliquus* biomass

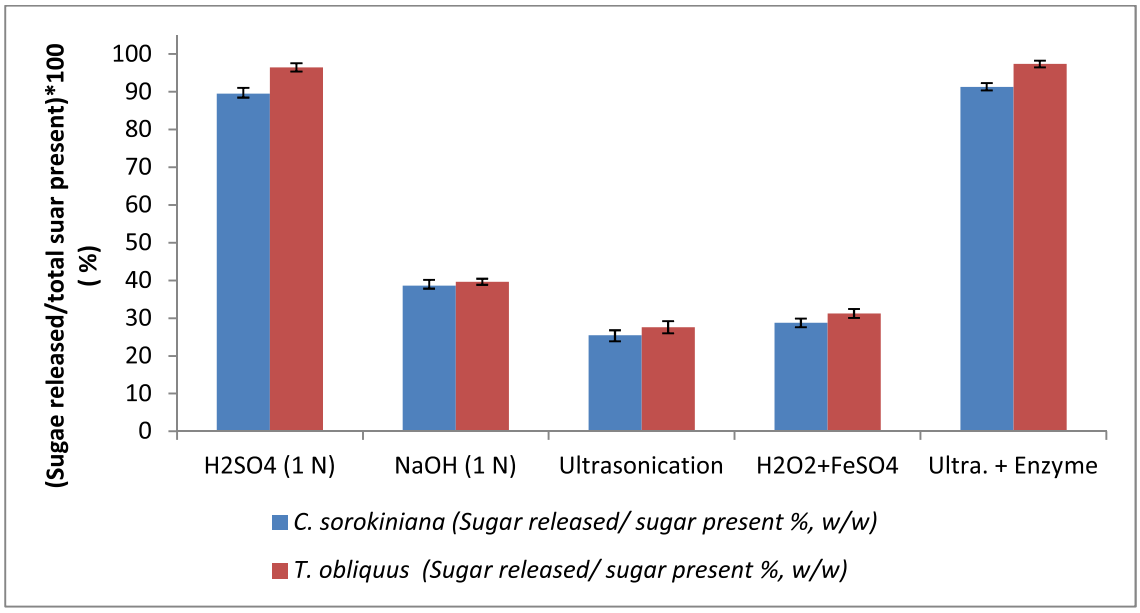

Fig. 4.36: The sugar released after pretreatment of *C. sorokiniana* and *T. obliquus* biomass by different pretreatment methods

4.4.7 SEM study of pretreated microalgal biomass

SEM analysis can be used to investigate the effects of pretreatments on microalgae cells. Both the microalgae, *C. sorokiniana* and *T. obliquus*, were analysed before and after the pretreatment under the scanning electron microscope to check the disruption of the cells. The results of SEM analysis are shown in Figure 4.37. In Figure 4.37 (A), an intact cell of *C. sorokiniana* can be seen without the pretreatment. The disrupted and ruptured cells of *C. sorokiniana* were obtained after the pretreatment which is shown in Figure 4.37 (B). Figure 4.37 (C) shows the intact cell of *T. obliquus* before the pretreatment. The broken and ruptured cells of *T. obliquus* can be seen in Figure 4.37 (D). SEM images indicate that in both cases, after pretreatment the cell wall was ruptured, and cellular contents came out of the cells which allowed the enzymes to easily access the carbohydrates to hydrolyse them. Enhanced hydrolysis may improve the productivity of the bioethanol.

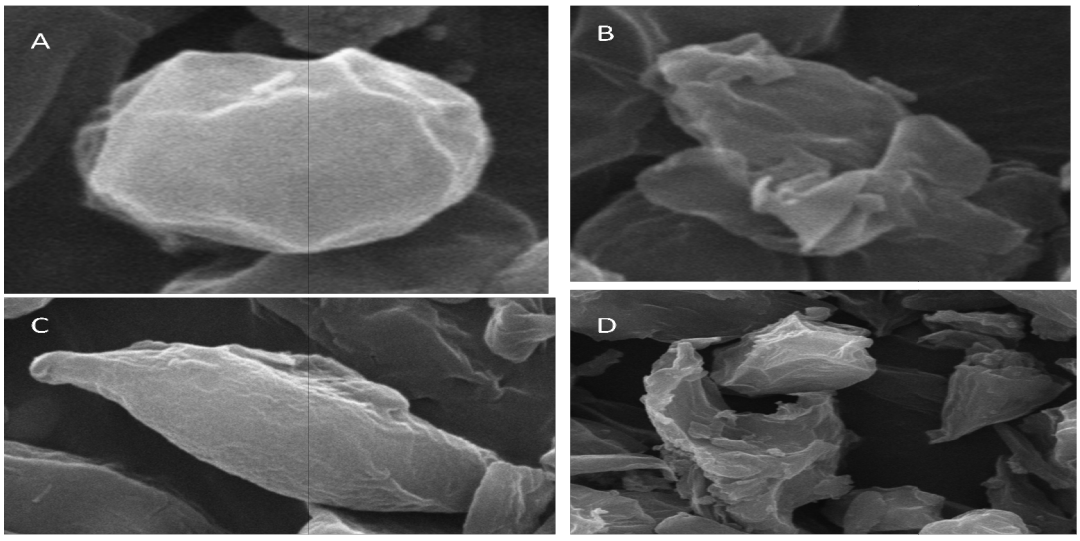

Fig. 4.37: The SEM images of *C. sorokiniana* (A- before pretreatment and B – after pretreatment) and *T. obliquus* (C- before pretreatment and D - after pretreatment)

Spiden *et al.* studied the cell rupturing of *Chlorella sp* and *Navicula* sp. by high-pressure homogenization after acidic and thermal treatment. The microalgae cells breakage was confirmed with SEM study (Spiden et al., 2015)

4.5 Fermentation of algal carbohydrate

Ethanol can be produced using carbohydrate mainly starch derived from microalgae through separate hydrolysis and fermentation (SHF) and simultaneous saccharification and fermentation (SSF). For the ethanol production from microalgae, ultrasonication followed by enzymatic pretreatment can be used as pretreatment strategy because the maximum sugar release was obtained with this pretreatment method. Since the sugar release after the acidic pretreatment is near to sugar released after the enzymatic pretreatment. Therefore, the ethanol productions after the acidic and enzymatic pretreatments of algal carbohydrate were compared.

4.5.1 Separate hydrolysis and fermentation (SHF) of microalgal carbohydrate

Separate hydrolysis and fermentation of algal carbohydrate were done in two-step process. In the first step, all the carbohydrate mainly starch is hydrolyzed into simple sugars by acidic or enzymatic hydrolysis and in the second step, the reducing sugars were utilized by yeast *Saccharomyces cerevisiae* for production of ethanol**.** The pretreatment/hydrolysis of microalgae was performed with 1 N sulphuric acid and ultrasonication followed by enzymatic treatment methods and both the methods were compared in terms of sugar yield and ethanol production.

4.5.1.1 Effect of biomass concentration on total sugar yield

Dilute acids hydrolyze carbohydrates/starch in the algal biomass to release simple sugars, which can be fermented into ethanol**.** The hydrolysis kinetics of algal biomass depends on the

type of biomass, temperature, acid concentration, and reaction time (Malester et al., 1988). The various concentrations (5, 10, 15, 20, 25 and 30 % (w/v)) of algal biomass were pretreated/ hydrolyzed by acidic (1 N H_2SO_4) pretreatment and ultrasonication followed by enzymatic pretreatment methods. Table 4.3 listed the amount of sugar released from both the microalgae using acidic and enzymatic (UFEP) pretreatment methods. The effect of biomass concentrations on total reducing sugars yield is shown in Figure 4.38. In acidic pretreatment as the concentration of microalgae biomass was increased from 5 to 25% (w/v), there was no significant change in the total sugar yield. However, as the concentration of microalgae biomass was increased from 25 to 30% (w/v), the total sugar yield reduced from 89.9 to 84.6% (w/v) and from 97.2 to 91.9% (w/v) in *C. sorokiniana* and *T. obliquus* respectively.

As the algal biomass concentration was increased from 5 to 25% (w/v) in UFEP method, there was no significant change in total sugar yield. However, as the algal biomass concentration was increased from 25 to 30% (w/v), the total sugar yield reduced from 91.8% to 88.6% and 97.5% to 93.1% in *C. sorokiniana* and *T. obliquus* respectively. The effect of algal biomass on total sugar yield through UFEP method is shown in Figure 4.39.

Microalgae biomass concentration is one of the significant factors, which can be optimized to obtain a high sugar yield. In current studies, 25 % (w/v) is found as the optimum value for getting the high amount of total sugar yield in the both acidic and enzymatic method.

4.5.1.2 Fermentation of reducing sugars to ethanol

After the pretreatment and hydrolysis, the total reducing sugars were fermented to produce ethanol by *Saccharomyces cerevisiae.* The total sugar yields obtained from acidic and

enzymatic pretreatment (UFEP) methods were nearly similar. The ethanol production yields were compared between acidic and UFEP methods in non-agitated and agitated conditions.

Table 4.3: Sugar released after acidic and UFE pretreatment methods

Algal biomass concentration % (w/v)	Acidic pretreatment		Enzymatic (UFEP) pretreatment	
	Sugar released using C. sorokiniana % (w/v)	Sugar released using T. obliquus % (w/v)	Sugar released using C. sorokiniana % (w/v)	Sugar released using T. obliquus % (w/v)
5	2.45	2.73	2.50	2.72
10	4.92	5.47	5.00	5.52
15	7.39	8.31	7.57	8.34
20	9.82	10.95	10.01	11.09
25	12.31	13.8	12.57	13.83
30	13.89	15.65	14.56	15.85

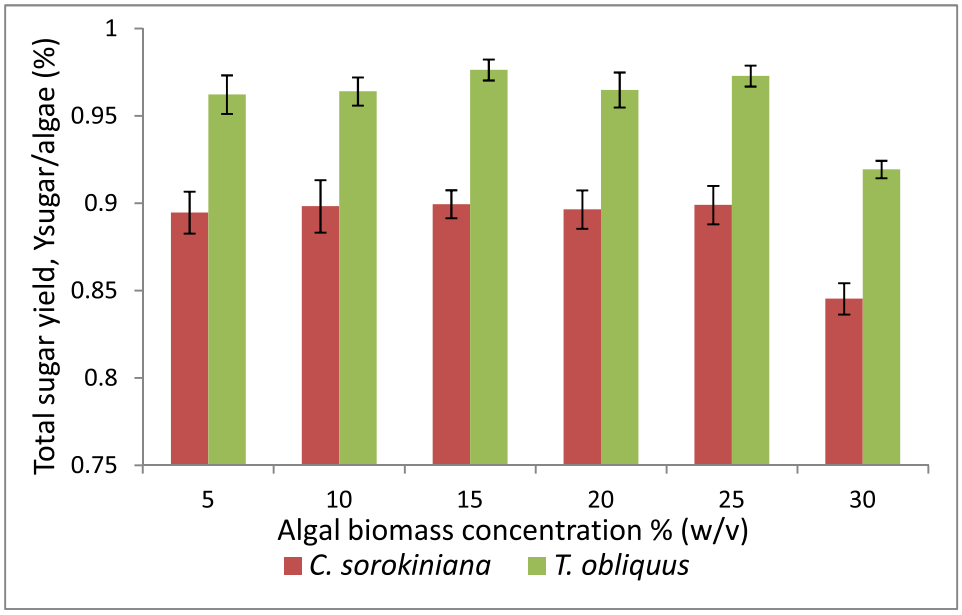

Fig. 4.38: The effect of biomass concentrations on total reducing sugar yield by acidic pretreatment

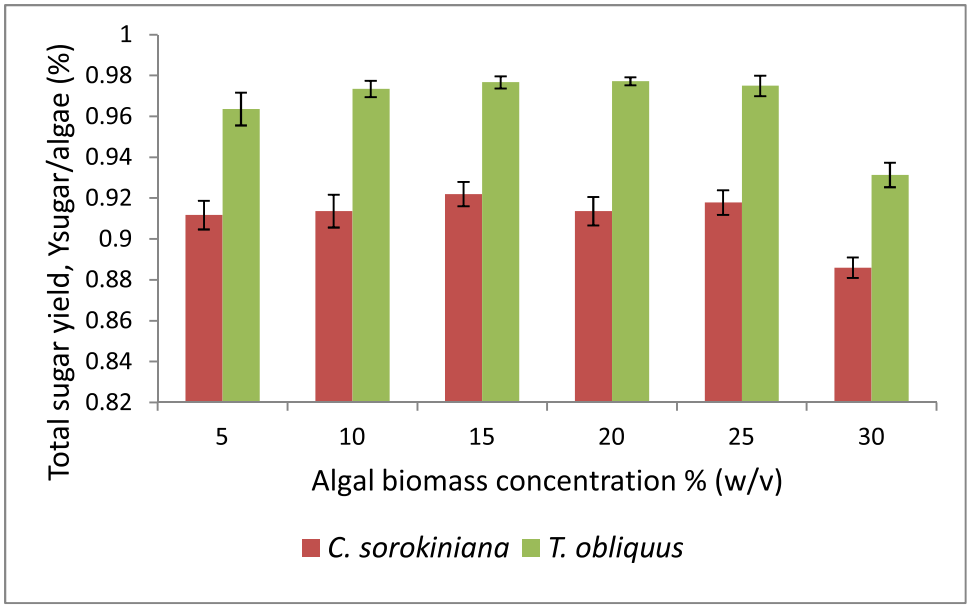

Fig. 4.39: The effect of biomass concentrations on total reducing sugar yield by ultrasonication followed by enzymatic pretreatment

4.5.1.3 SHF under the non-agitated condition

The initial sugar concentrations of *C. sorokiniana* biomass were measured after the enzymatic and acidic hydrolysis as 12.6 and 12.3 % (w/v) respectively. Figure 4.40 shows the fermentation profile of reducing sugars and ethanol production under non-agitated condition from acidic and enzymatic hydrolyzed biomass of *C. sorokiniana*. After the 64 hours of fermentation, *S. cerevisiae* rapidly consumed the sugars resulting in an increase of ethanol concentration and reduction in sugar concentrations, which were found as 0.323 and 1.016 % (w/v) for enzymatic (UFEP) and acidic hydrolysis respectively. The ethanol productions were measured as 4.0 and 2.95% (w/v) for enzymatic (UFEP) and acidic hydrolysis respectively. The ethanol yields were obtained as 0.325 and 0.245 (g of ethanol/g of carbohydrate) for enzymatic (UFEP) and acidic hydrolysis respectively. The ethanol production in case of enzymatic (UFEP) hydrolysis was found higher than acid hydrolysis

because some of the inhibitory products are formed during pretreatment and hydrolysis which inhibit the growth of yeast cells and reduces the ethanol production.

T. obliquus biomass provided the initial sugar content as 13.83 and 13.8% (w/v) after enzymatic (UFEP) and acidic hydrolysis respectively. The ethanol fermentation profile of acidic and enzymatic hydrolyzed biomass of *T. obliquus* under non agitated condition is shown in Figure 4.41. After 64 h of fermentation, the sugar was utilized by the yeast for the production of ethanol and reduced to 0.36 and 1.26% (w/v) for enzymatic (UFEP) and acidic hydrolysis respectively. The ethanol production was found as 4.43 % and 3.31% (w/v) from *T. obliquus* biomass by enzymatic (UFEP) and acidic hydrolysis respectively. The ethanol yields were obtained as 0.328 and 0.263 (g of ethanol/g of carbohydrate) for enzymatic (UFEP) and acidic hydrolysis respectively.

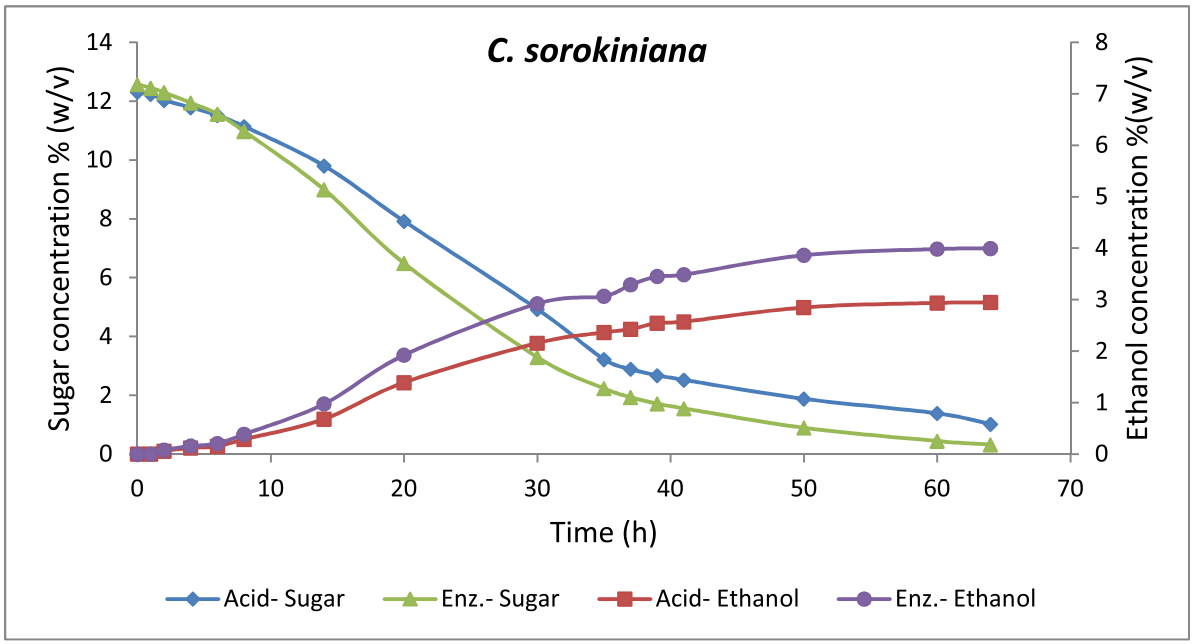

Fig. 4.40: The sugar depletion and ethanol production profiles of SHF in *C. sorokiniana* biomass after acidic and enzymatic hydrolysis (UFEP) under non-agitated condition

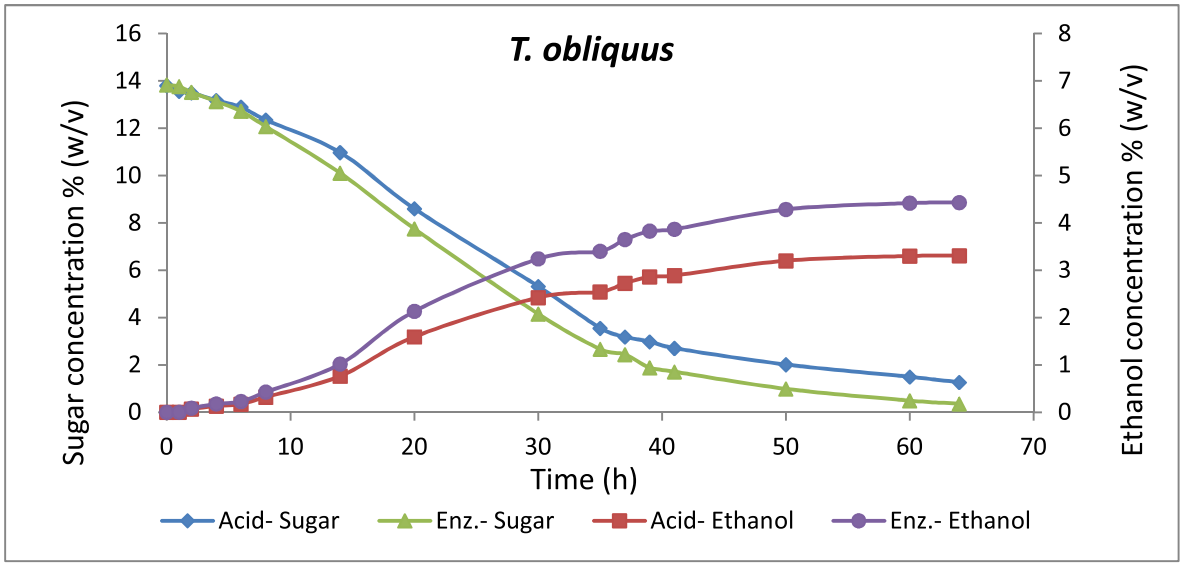

Fig. 4.41: The sugar depletion and ethanol production profiles of SHF using *T. obliquus* biomass after acidic and enzymatic hydrolysis under the non-agitated condition

4.5.1.4 SHF under the agitated condition

Figure 4.42 shows the ethanol fermentation of hydrolyzed carbohydrates of *C. sorokiniana* under agitated condition. The initial sugar concentrations of *C. sorokiniana* biomass were measured as 12.6 and 12.3 % (w/v) after the enzymatic (UFEP**)** and acidic hydrolysis respectively. The rate of sugar consumption by yeast cells under agitated condition was higher than the non-agitated condition. After the fermentation, the residual sugar concentrations were measured as 0.7 and 0.21% (w/v) for acidic and enzymatic (UFEP**)** hydrolysis respectively. The ethanol productions were measured as 5.31 and 4.07 % (w/v) for enzymatic and acidic hydrolysis respectively. The ethanol yields were obtained as 0.428 and 0.342 (g of ethanol/ g of carbohydrate) for enzymatic (UFEP) and acidic hydrolysis respectively. The ethanol production was higher in agitated condition than non- agitated condition.

Similarly, the ethanol fermentation was performed in reducing sugar obtained from *T. obliquus* after acidic and enzymatic hydrolysis as shown in Figure 4.43. The initial sugar concentrations obtained after enzymatic and acidic hydrolysis were measured as 13.83 and 13.8 % (w/v) respectively. The rate of sugar consumption by yeast cells was higher in case of enzymatic hydrolysis than acidic hydrolysis because in acidic hydrolysis some of the inhibitory compounds are formed which inhibit the growth and production of ethanol. The sugar concentrations reduced to 0.68 and 0.23% (w/v) after fermentation in acidic and enzymatic hydrolysis respectively. The ethanol productions were found as 5.96 and 4.59% (w/v) and ethanol yields were observed 0.438 and 0.349 (g of ethanol / g of carbohydrate) for enzymatic and acidic hydrolysis respectively. The by-products of the acidic pretreatment, which are produced by the oxidation of sugars into furfural and hydroxymethylfurfural, inhibit the growth of the microorganism and also interfere during the ethanol production.

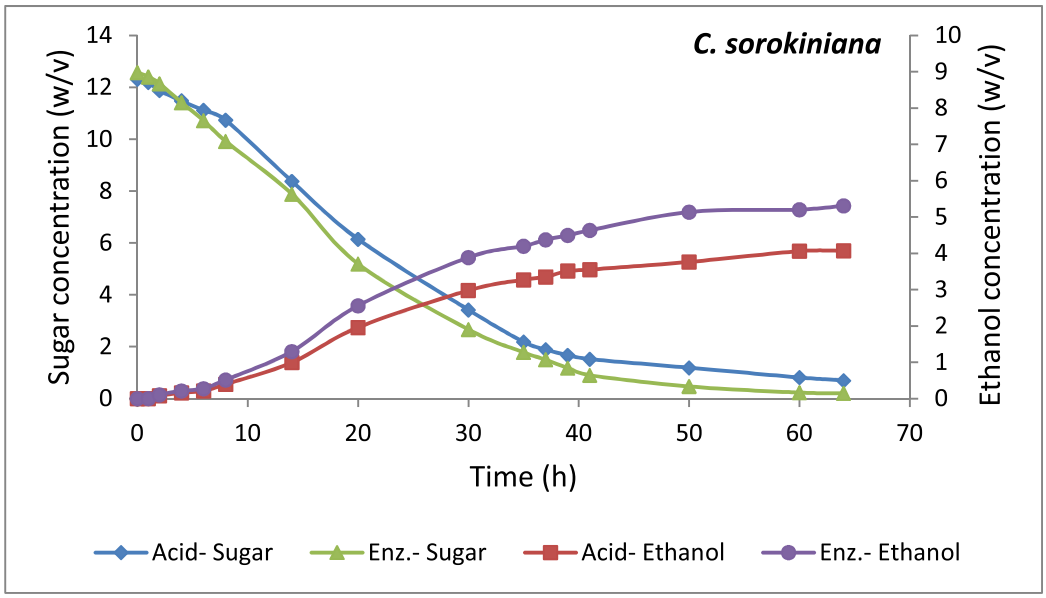

Fig. 4.42: The sugar depletion and ethanol production profiles of SHF using *C. sorokiniana* biomass after acidic and enzymatic (UFEP) hydrolysis under the agitated condition

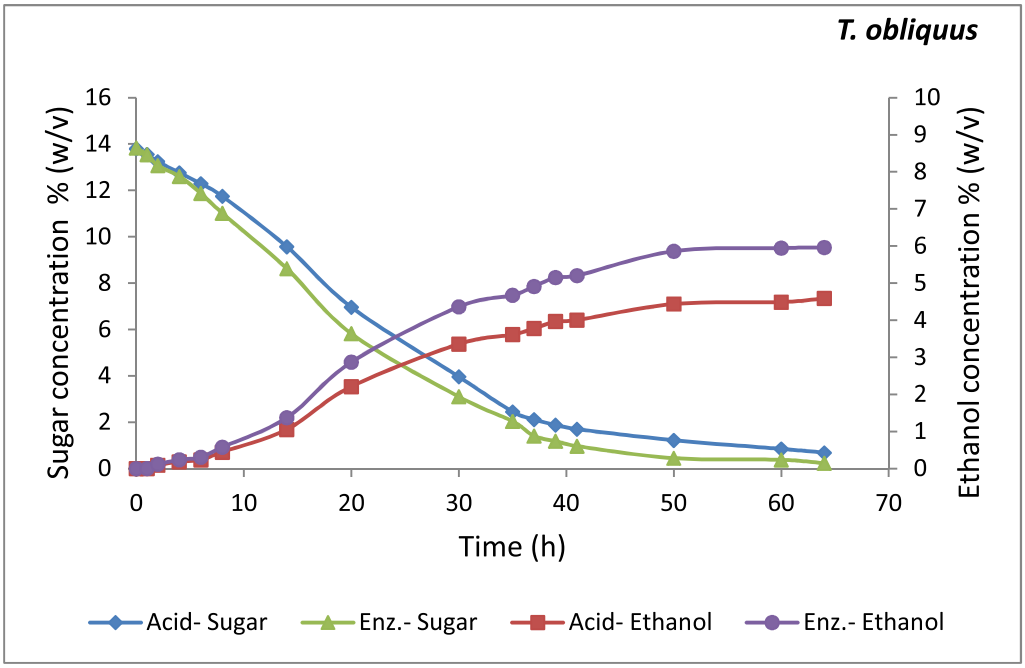

Fig. 4.43: The sugar depletion and ethanol production profiles of SHF using *T. obliquus* after acidic and enzymatic hydrolysis (UFEP) under the agitated condition

Shokrkar *et al* (2017) reported that acidic and enzymatic pretreatments provided the approximate similar amount of sugar release from microalgae biomass. However, the ethanol production from enzymatic pretreatment was higher 0.46 (g/ g of glucose) than acidic pretreatment i.e. 0.38 (g/g of glucose) (Shokrkar et al., 2017). Therefore, ultrasonication followed by enzymatic pretreatment (UFEP**)** was chosen as a pretreatment strategy for the microalgae biomass for the production of ethanol.

4.5.2 Simultaneous saccharification and fermentation (SSF) of microalgal carbohydrate

Ultrasonicated treated microalgae biomass was used as a substrate for SSF. In SSF, microalgae carbohydrate is hydrolyzed to fermentable sugar by a group of enzymes. After the hydrolysis, the reducing sugars are used for ethanol production by *S. cerevisiae*. Ethanol

fermentation was performed under agitated and non agitated conditions using both treated *C. sorokiniana* and *T. obliquus* biomass.

4.5.2.1 SSF of microalgal carbohydrate under the non-agitated condition

Figure 4.44 shows the profiles of total carbohydrate (like cellulose and starch) depletion, glucose accumulation and ethanol production during simultaneous saccharification and fermentation of carbohydrates obtained from *C. sorokiniana.* The initial total carbohydrate was measured as 12.57% (w/v). The carbohydrates like cellulose and starch are hydrolyzed to glucose by the enzymes and produced glucose is simultaneously utilized by yeast, *S. cerevisiae,* cells for their growth and production of ethanol. After the fermentation, total carbohydrate reduced to 0.166% (w/v). The initial glucose accumulation which reached to its maximum concentration as 2.0% (w/v) after 8 h of fermentation was due to higher glucose production as compared to its consumption. Since after the 10 h, the rate of glucose consumption was higher than glucose generation, therefore, a depletion profile of glucose was observed and reduced to 0.08% (w/v). The ethanol production was initially very slow but as the concentration of yeast cells increased, the ethanol production is also increased and reached to its maximum level as 3.83% (w/v) after 64 h. The ethanol yield was found as 0.307 (g of ethanol /g of carbohydrate)

The fermentation profile of SSF using *T. obliquus* carbohydrate is shown in Figure 4.45. The initial carbohydrate was measured as 13.83% (w/v). As the fermentation proceeded, the reduction in carbohydrate content was observed and reached 0.09% (w/v) after 64 h of fermentation. The glucose concentration accumulated in the process and reached its maximum concentration as 2.01% (w/v) after 8 h of fermentation. After 8 h, the rate of glucose generation was lower than glucose consumption and therefore its depletion profile

was observed. The ethanol concentration was initially very low however as the fermentation proceeded its concentration reached to maximum concentration as 4.18% (w/v) at the end of the fermentation. . The ethanol yield was found as 0.308 (g of ethanol /g of carbohydrate).

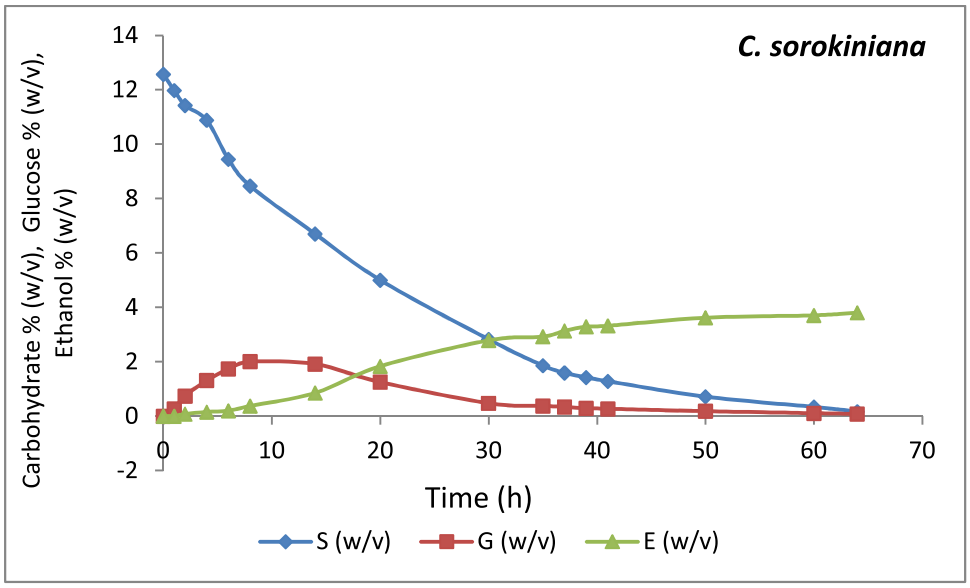

Fig. 4.44: Concentration profiles of carbohydrate (*S*), glucose (*G*), and bioethanol (*E*) of SSF using *C. sororkiniana* biomass under non-agitated condition

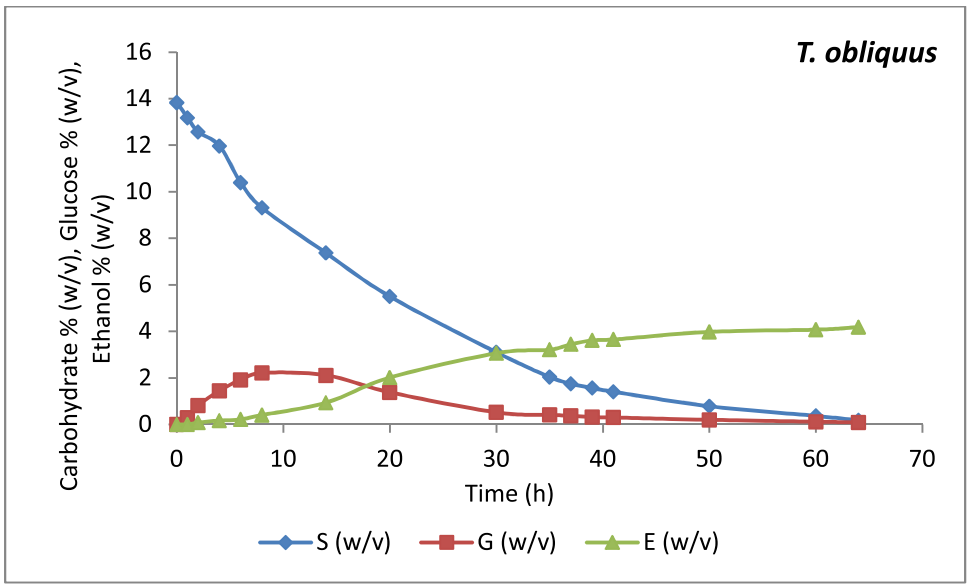

Fig. 4.45: Concentration profiles of carbohydrate (*S*), glucose (*G*), and bioethanol (*E*) of SSF using *T. obliquus* biomass under the non-agitated condition

4.5.2.2 SSF of microalgal carbohydrate under the agitated condition:

The SSF profile of carbohydrate of microalgae *C. sorokiniana* under shaking condition is shown in Figure 4.46. The algal carbohydrate is hydrolyzed into reducing the sugar by a mixture of enzymes and simultaneously glucose is utilized by yeast *S. cerevisiae* for production of ethanol. The rate of carbohydrate hydrolysis was comparatively higher during the initial period of fermentation. The initial carbohydrate content was measured as 12.57% (w/v) and almost all the carbohydrate was depleted after 40 h of fermentation. Liu *et al.* and Lee *et al*. also observed a similar trend of decrease in starch concentrations (Lee et al., 1992; Liu et al., 2014). The starch depletion profile mainly depends on the activity of amylase enzyme and capability of the microorganism to utilize the reducing sugars.

In the fermentation broth, the rise in glucose concentration was observed in the early period of fermentation, and the highest accumulated glucose concentration was found as 1.82 % (w/v) after 8 h of fermentation and further glucose concentration was decreased and reached to its minimum concentration after 64 h of fermentation. The increase in glucose concentration was noticed because the rate of glucose formation was initially higher than its rate of consumption. In the later stage, the decline in glucose concentration was observed because the rate of glucose formation was lower than its utilization. The rapid increase in reducing sugar level due to starch hydrolysis followed by a slow decreasing pattern of reducing sugar concentration due to fermentation was also observed in the study performed by Lee *et al.* (Lee et al., 1992; Liu et al., 2014).

In the initial period of fermentation, no significant amount of ethanol was estimated, but after 4 hours, ethanol concentration increases continuously till 50 hours. The ethanol concentration was measured as 0.57% (w/v) after 8 h of fermentation and increased as fermentation

proceeded and reached to its maximum concentration of 5.82% (w/v). The ethanol yield was found as 0.463 (g of ethanol / g of carbohydrate).

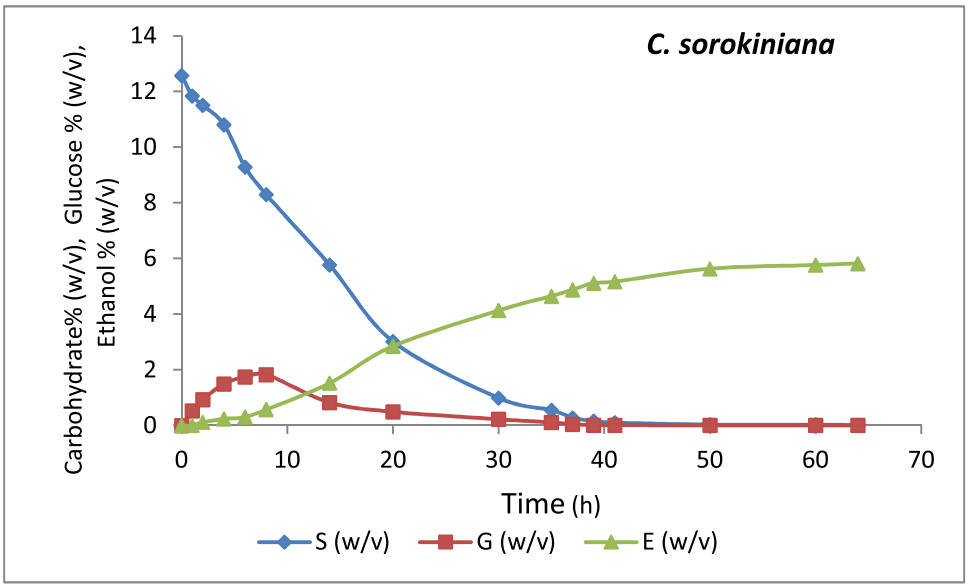

Fig. 4.46: Experimental concentration profiles of carbohydrate (*S*), glucose (*G*), and bioethanol (*E*) vs time (t) of SSF using *C. sororkiniana* biomass under the agitated condition

The ethanol production in SSF under shaking condition from *C. sorokiniana* was higher than the non-agitated condition. Kadar *et al.* compared the production of ethanol from industrial waste through SSF by *S. cerevisiae* and a thermotolerant strain *K. marxianus*. They found the ethanol production in the range of 0.31-0.34 g/g for both the strain (Kádár et al., 2004). The results obtained here are in well accordance with the study conducted by Chandel *et al.* (2010) who reported 15.73 g/l ethanol with the yield 0.42 g/g at pH- 6.4, temperature 28°C from *Pichia stipitis* NCIM3498 (Chandel et al., 2010).

Figure 4.47 shows the SSF of *T. obliquus* carbohydrate under shaking condition. The initial carbohydrate was measured 13.83% (w/v) for the SSF process. The depletion of carbohydrate concentration could be seen as it was hydrolyzed into reducing sugar and further used by yeast cells. The hydrolyzed carbohydrate formed the glucose and its concentration increased till the rate of glucose generation was higher than it consumption. The glucose concentration reached its maximum concentration of 2.0% (w/v) and further decreased as utilized by *S.*

cerevisiae for production of ethanol. The ethanol production was initially very low but as fermentation process proceeded its concentration reached its maximum level as 6.43% (w/v). The ethanol yield was found as 0.465 (g of ethanol/ g of carbohydrate). The comparative ethanol production yield of different processes of SHF and SSF are reported in Table 4.3 (a).

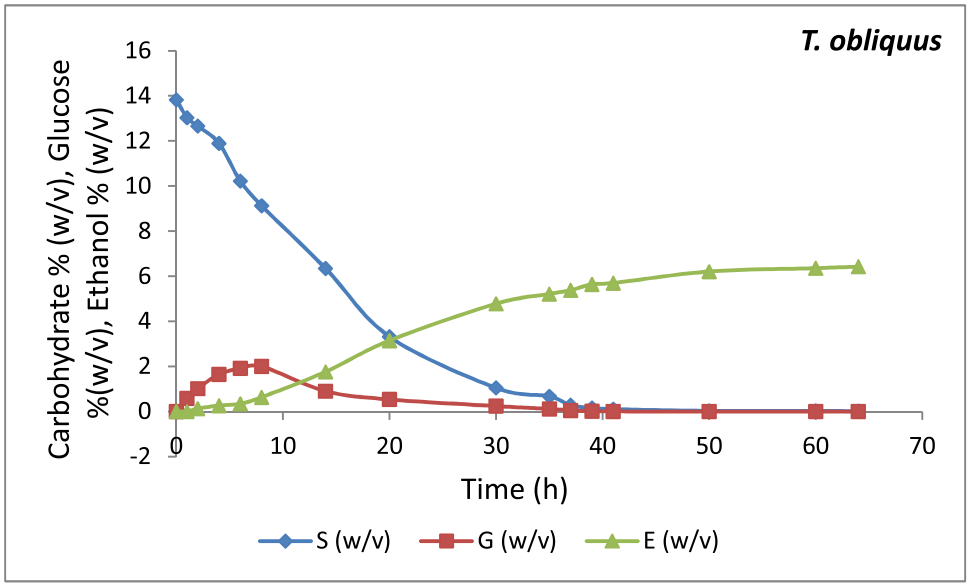

Fig. 4.47: Experimental concentration profiles of carbohydrate (*S*), glucose (*G*), and bioethanol (*E*) vs time (t) of SSF using *T. obliquus* under the agitated condition

Table 4.3 (a): The comparative ethanol yield obtained from different processes of SHF and SSF

Carbohydrate obtained from	Ethanol Yield (g of ethanol/g of carbohydrate) in SHF		Ethanol Yield (g of ethanol/g of carbohydrate) in SSF	
	Non-agitated	Agitated	Non-agitated	Agitated
C. sorokiniana	0.325±0.01	0.428±0.011	0.307±0.009	0.463±0.012
T. obliquus	0.328±0.011	0.438±0.008	0.308±0.015	0.465±0.014

4.5.3 Mathematical modelling of SHF under non-agitated and agitated conditions

Since the maximum ethanol production was obtained with the *T. obliquus* biomass with enzymatic hydrolysis and therefore for the mathematical modelling of SHF, fermentation data of *T. obliquus* was taken for further study. The SHF profiles of ethanol fermentation

using *T. obliquus* under non-agitated and agitated conditions are shown in Figure 4.48 and 4.52 respectively. Mathematical model equations have been used to mimic the physical behaviour of SHF. The unknown parameters in models were calculated by minimizing the normalized error among kinetic data with model data by using solver function of MS Excel (Microsoft Corporation Redmond, WA, USA). The different kinetic constants of model equations for SHF under non-agitated and agitated condition are evaluated and listed in Table 4.4.

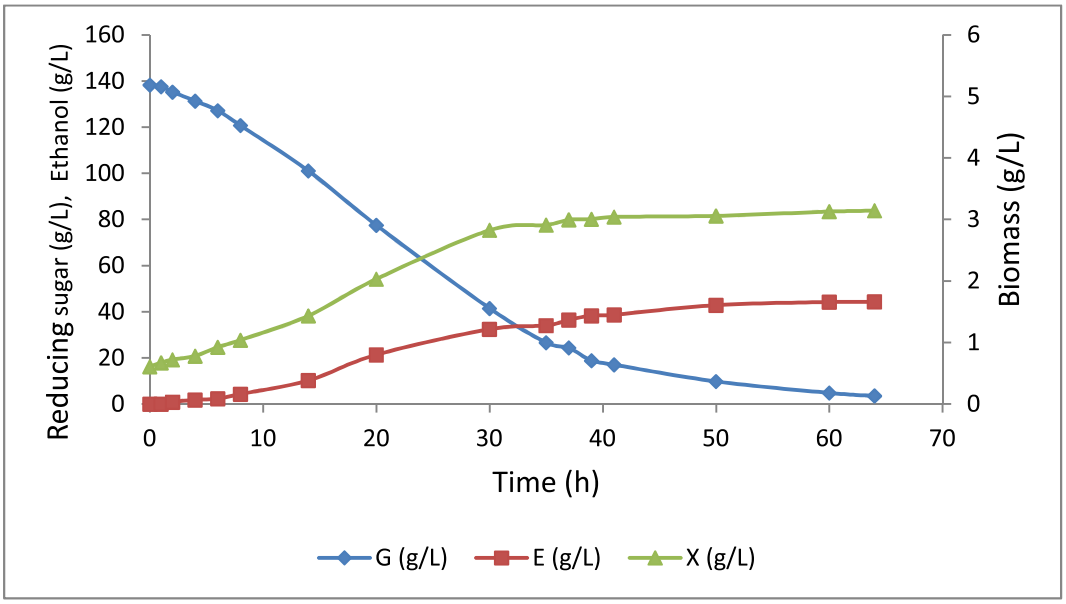

Fig. 4.48: The concentration profiles of reducing sugar (*G*), yeast cell mass (*X*) and ethanol (*E*) during SHF under the non-agitated condition

From the experimental data, four constants, X_{max}, μ_{max}, $Y_{X/S}$ and m_s in model equations were evaluated, and the sugar depletion profile can be predicted using Pirt's equation (Soto-Cruz et al., 2002). The predicted and experimental profiles of reducing sugar concentration under the non-agitated and agitated condition of fermentation are shown in Figure 4.49 and 4.53 respectively.

Table 4.4: Values of constants used in the model equations for SHF under agitated and non-agitated condition

Kinetic parameters	Units	Non-agitated	Agitated
X_{max} (Maximum cell mass concentration)	gL^{-1}	3.22	5.02
μ_{max} (Maximum specific growth rate)	h^{-1}	0.102	0.129
$Y_{X/S}$ (Cell mass yield coefficient)	gg^{-1}	0.021	0.033
m_s (maintenance coefficient)	$gg^{-1}h^{-1}$	0.016	0.005
α (growth-associated coefficient for the product)	gg^{-1}	13.418	8.35
β (non-growth-associated coefficient for the product)	$gg^{-1}h^{-1}$	0.411	0.154

In non-agitated SHF, the experimental values of reducing sugars were higher compared to predicted values in an initial period of fermentation. In the later period of SHF, the predicted values of glucose concentration were similar to the experimental values. In the agitated condition of SHF, the predicted values of glucose concentration were very close to the experimental values. The coefficients of determination (R^2-values) for different models are given in Table 4.5. The calculated R^2 values between predicted and experimental values of reducing sugar concentration were found as 0.98 and 0.997 under non-agitated and shaking condition of fermentation respectively.

The cell growth of *S. cerevisiae* in SHF process was predicted by logistic equation. Two parameters maximum cell concentration (X_{max}) and specific growth rate (μ) were calculated experimentally. Figure 4.50 and 4.54 show the growth profile of *S. cerevisiae* under non-agitated and agitated conditions of fermentation respectively. The results show that the maximum yeast cell biomass concentration achieved were 3.04 and 4.88 g/L under non-

agitated and shaking condition respectively. The R^2-values between predicted and experimental values of cell mass under non-agitated and shaking condition of fermentation were found as 0.995 and 0.983 respectively.

Table 4.5: Coefficient of determination (R^2) for different models

Predicted models for	Models	R^2- values	
		Nonagitated	Agitated
Glucose	$G(X) = G_0 - \frac{1}{Y_{x/s}}(X - X_0) - \frac{m.X_{ma}}{\mu}\ln\left(\frac{X_{ma} - X_0}{X_{ma} - X}\right)$	0.98	0.997
Cell mass	$X(t) = \frac{X_{ma}}{1 + \left(\frac{X_{ma}}{X_0} - 1\right)e^{-\mu t}}$	0.995	o.983
Ethanol	$E(X) = E + \alpha(X - X_0) + \frac{\beta.X_{ma}}{\mu}\ln\left(\frac{X_{ma} - X_0}{X_{ma} - X}\right)$	0.991	0.964

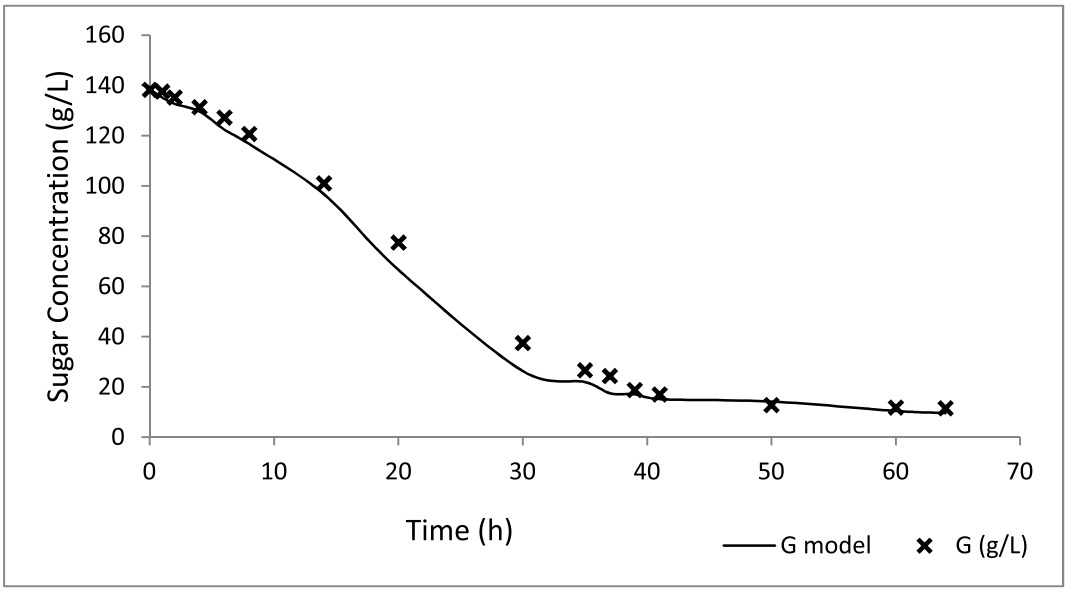

Fig. 4.49: The experimental and predicted profiles of reducing sugar consumption during SHF under non-agitated condition. Line (---) shows the model data and cross (×) shows the experimental data

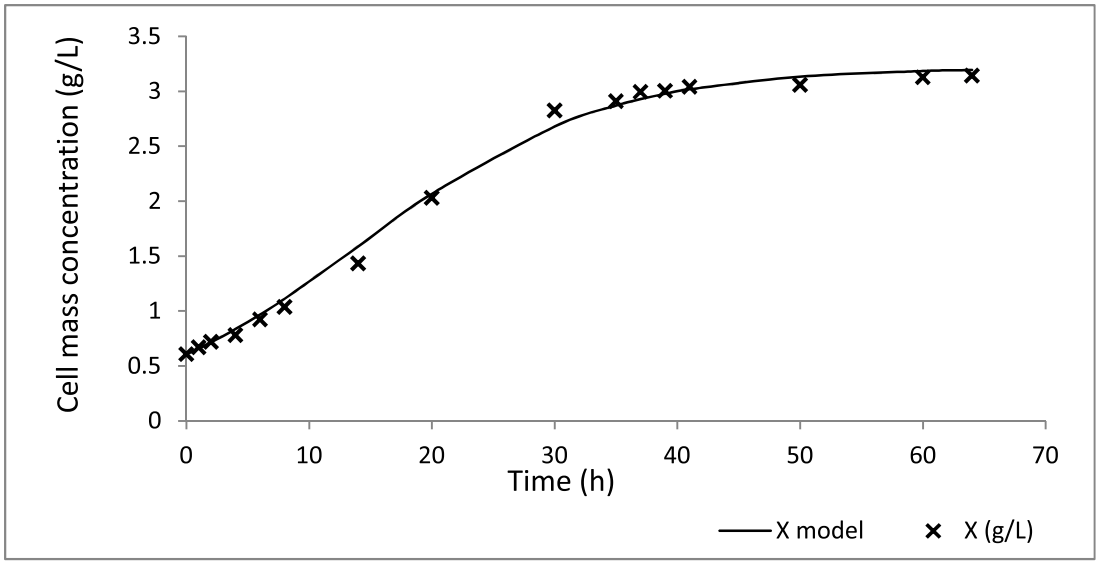

Fig. 4.50: The experimental and predicted profiles of yeast cell mass generation during SHF under non-agitated condition. Line (---) shows the model data and cross (×) shows the experimental data

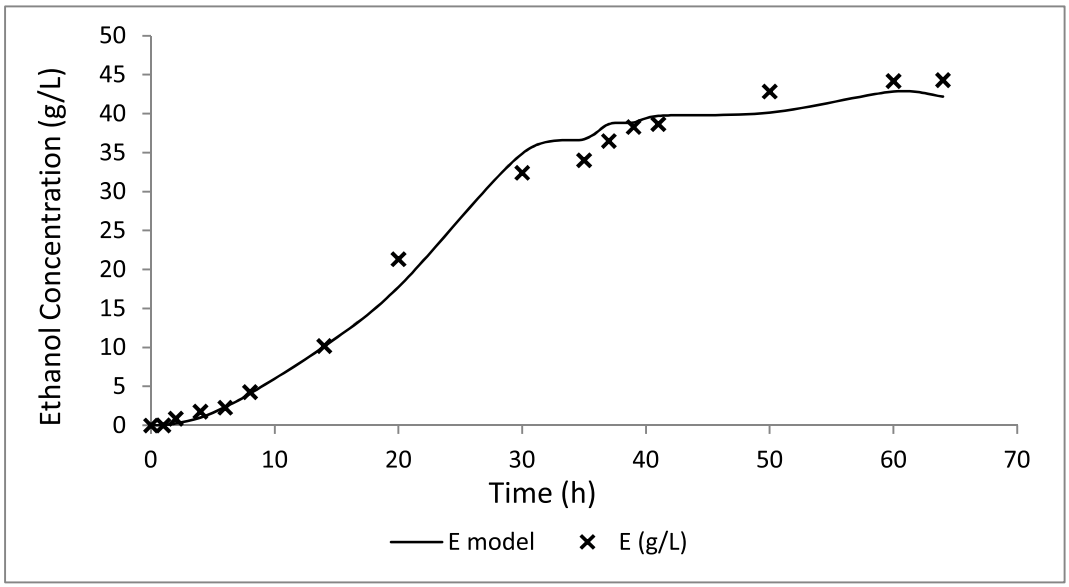

Fig. 4.51: The experimental and predicted profiles of ethanol production during SHF under non-agitated condition. Line (---) shows the model data and cross (×) shows the experimental data

The predicted and experimental values of ethanol concentration under the non-agitated and shaking condition of SHF are shown in Figure 4.51 and 4.55 respectively. In non-agitated fermentation condition, the predicted values of ethanol were slightly lower than experimental values during exponential phase. In shaking condition of SHF fermentation, the predicted values of ethanol were slightly lower than experimental values during exponential phase. However, in the deceleration phase, the predicted values of ethanol concentration were higher than the predicted values and later stage experimental values were higher than predicted values. The R^2 value between predicted and experimental values of ethanol concentration was found as 0.998 and 0.964 under non-agitated and shaking condition of fermentation respectively.

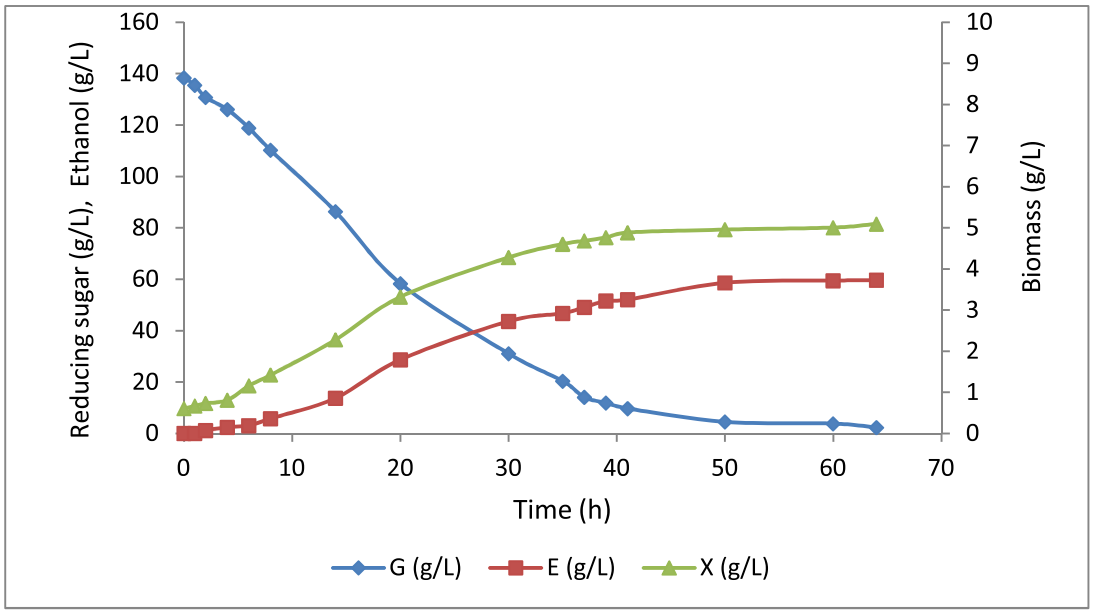

Fig. 4.52: The concentration profiles of reducing sugar (*G*), yeast cell mass (*X*) and ethanol (*E*) during SHF under agitated condition

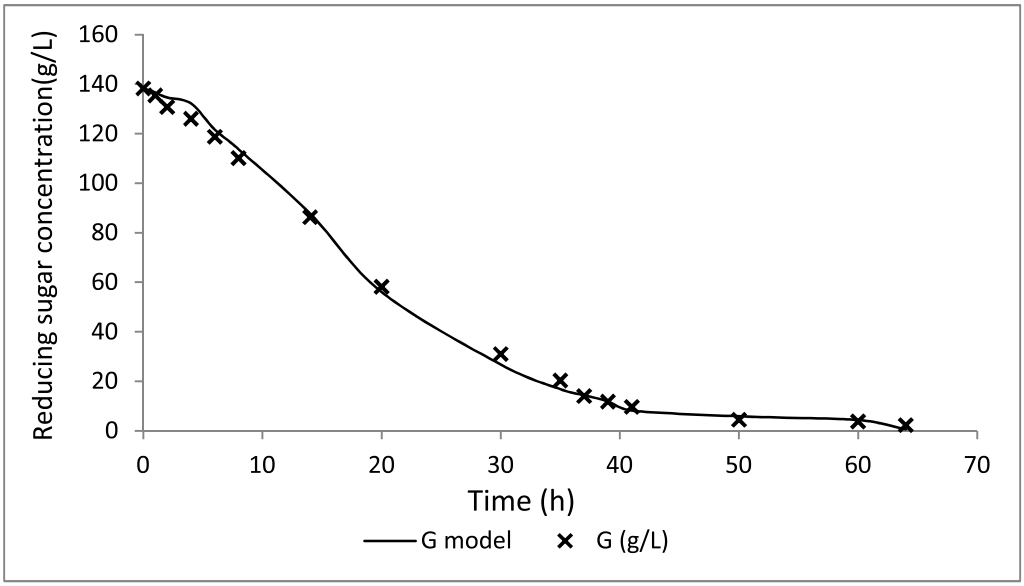

Fig. 4.53: The experimental and predicted profiles of reducing sugar consumption during SHF under shaking condition. Line (---) shows the model data while cross (×) shows the experimental data

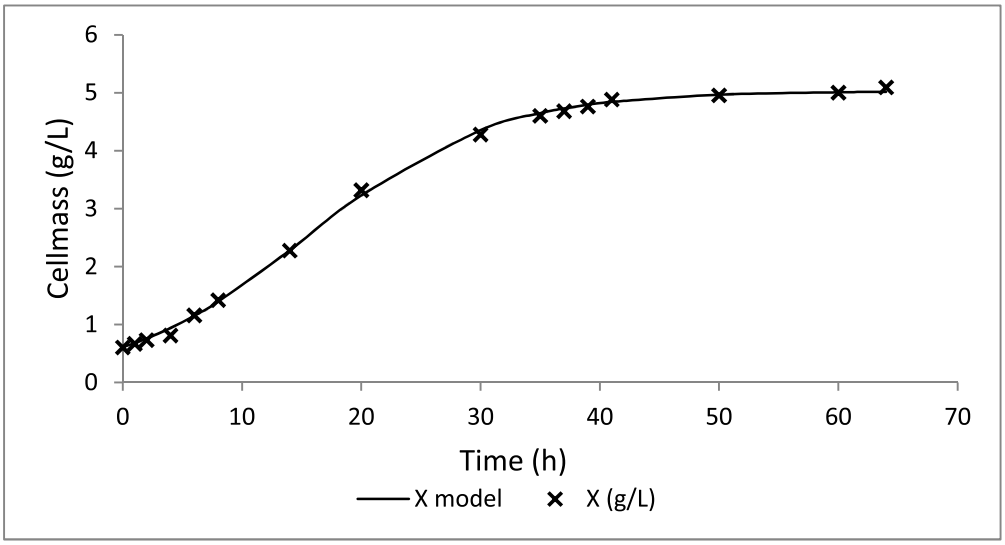

Fig. 4.54: The experimental and predicted profiles of yeast cell mass generation during SHF under shaking condition. (Line (---) shows the model data and cross (×) shows the experimental data)

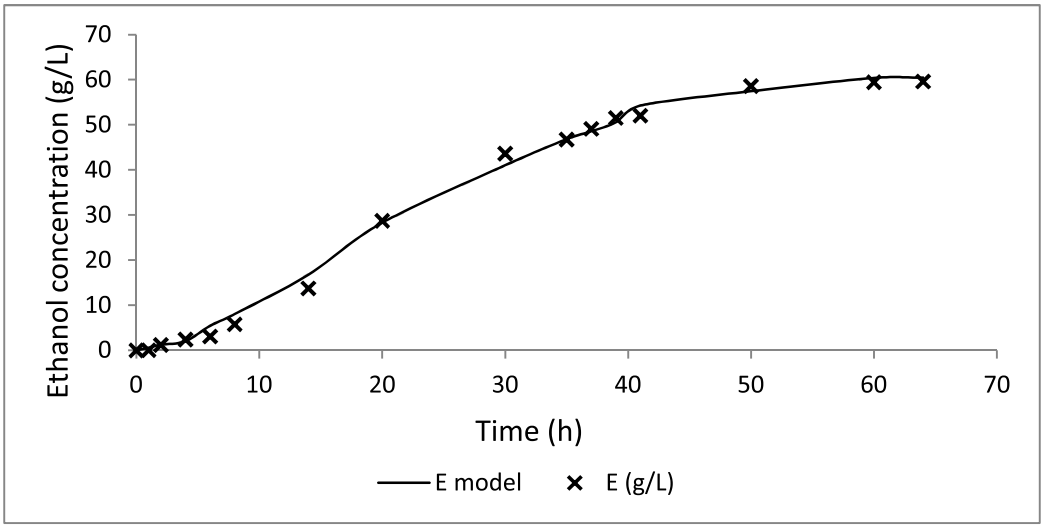

Fig. 4.55: The experimental and predicted profiles of ethanol production during SHF under shaking condition. (Line (---) shows the model data and cross (×) shows the experimental data)

4.5.4 Mathematical modelling of SSF of algal carbohydrate under non-agitated and agitated conditions

The SSF fermentation profiles of different parameters i.e. carbohydrate content, glucose concentration, yeast cell mass concentration and ethanol concentration under non-agitated and agitated conditions are shown in Figure 4.56 and 4.61 respectively. The yeast culture having a concentration of 0.609 g/L was used as inoculum. Initially, there was a lag period of cell growth for about 3 hours because the cells were adjusted itself for a new environment (Eklund and Zacchi, 1995). The yeast cells grew in the exponential phase with the maximum specific growth rate of 0.195 and 0.238h^{-1} under the non-agitated and agitated condition of fermentation. The cell mass concentration reached to stationary phase after 50 hours of fermentation. The maximum biomass concentrations were 3.32 and 5.37g/L under non-agitated and shaking condition of fermentation respectively. Liu *et al*. observed the

similar pattern of cell growth during the SSF of rice carbohydrate by *S. cerevisiae,* and the highest biomass was achieved as 5.2 g/L in 80h at 26^{o}C (Liu et al., 2014).

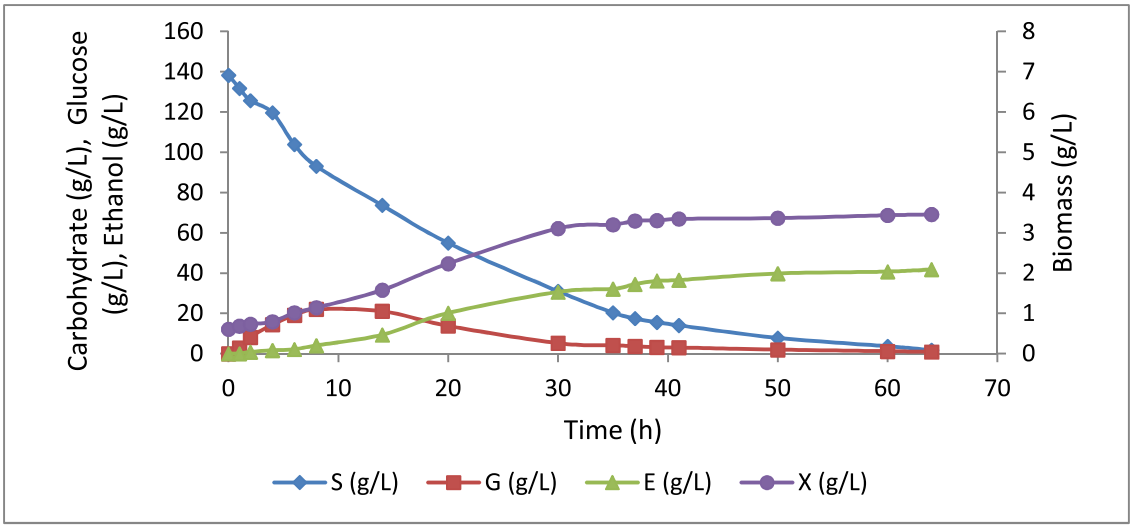

Fig. 4.56: The concentration profiles of glucose (*G*), carbohydrate (*S*) and ethanol (*E*) and yeast cell mass (*X*) during SSF

Different parameters in model equations were evaluated first to obtain glucose concentration, ethanol production and cell growth profiles in the SSF process, because *X, G*, and *E* are interdependent parameters. However, the carbohydrate content depends on the enzyme reaction velocity and its affinity towards the substrate. The unknown parameters in models were calculated by minimizing the normalized error among kinetic data with model data by using solver function of MS Excel (Microsoft Corporation Redmond, WA, USA). The list of evaluated constants for SSF under non-agitated and agitated conditions is shown in Table 4.6. The proposed model equations were solved using Polymath Educational software 6.1. The experimental data and data generated by models were analyzed statistically using the regression curve fitting with statistical significance at p =0.05 (Jiménez-Islas et al., 2014).

From the experimental data, two constants, k_m and V_m, in the model equation was evaluated, and carbohydrate depletion profile can be predicted using integration of differential equation of carbohydrate. The predicted and experimental profiles of carbohydrate concentration under the non-agitated and agitated condition of fermentation are shown in Figure 4.57 and 4.62 respectively. The coefficients of determination (R^2-values) for different models of SSF are given in Table 4.7. The calculated R^2 between predicted and experimental values of carbohydrate concentration was found as 0.998 and 0.997 under non-agitated and shaking condition of fermentation respectively. Thus, results indicate that a given model can predict experimental values.

Table 4.6: Values of constants used in the model equations for SSF under the agitated and non-agitated condition

Constants	Units	Non-agitated	Agitated
V_m	$gL^{-1}h^{-1}$	5.16	5.99
μ_m	h^{-1}	0.195	0.238
S_o	gL^{-1}	138.3	138.3
X_o	gL^{-1}	0.609	0.609
$Y_{X/S}$	gg^{-1}	0.027	0.041
$Y_{P/S}$	gg^{-1}	0.329	0.477
m_s	$gg^{-1}h^{-1}$	0.247	0.089
q_m	$gL^{-1}h^{-1}$	1.29	3.09
K_m	gL^{-1}	21.67	18.66
K_s	gL^{-1}	38.88	28.47
K_a	gL^{-1}	78.0	63.65

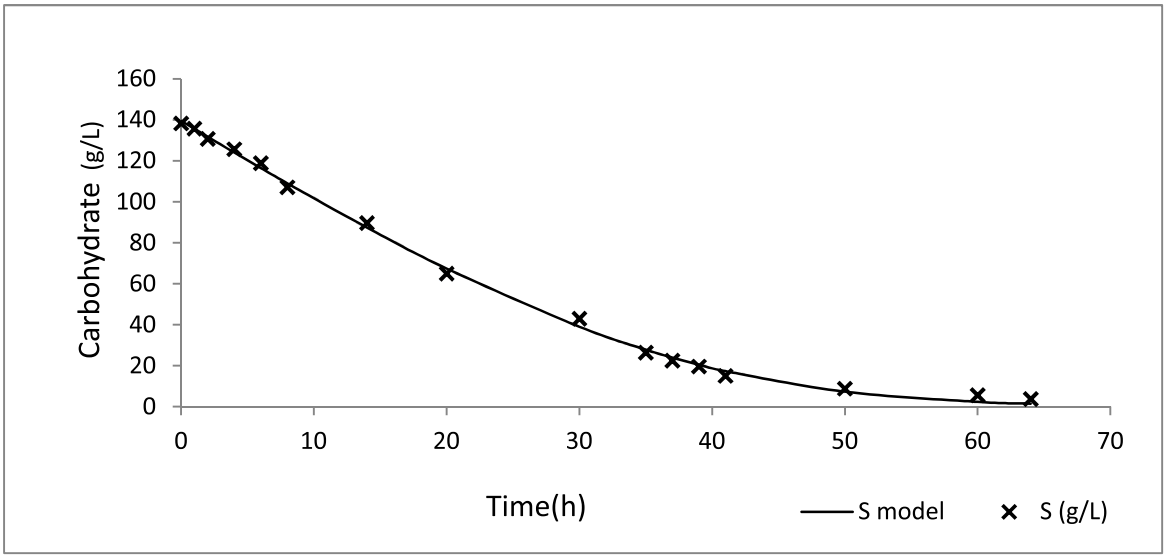

Fig. 4.57: Profile of predicted (lines) and experimental (×) carbohydrate depletion during the simultaneous saccharification and fermentation (SSF) process under the non-agitated condition

The predicted and experimental values of glucose concentration under the non-agitated and shaking condition of fermentation are compared and presented in Figure 4.58 and 4.63 respectively. In the non-agitated condition of fermentation, the rapid increase in glucose concentration was observed in both experimental and predicted values of the SSF process. However, the experimental values were higher compared to predicted values. In the later period of SSF, the predicted values were slightly lower than experimental values. In the agitated condition of fermentation, similar trends of glucose concentration for predicted and experimental values were observed as in non-agitated condition. The R^2 value between predicted and experimental values of glucose concentration was calculated as 0.914 and 0.935 under non-agitated and shaking condition of fermentation respectively.

The cell growth of *S. cerevisiae* in the SSF process was predicted by solving the differential equation for cell mass. Two parameters μ_m and k_s were calculated experimentally. The

experimental and predicted values of yeast cell growth are shown in Figure 4.59 and 4.64 under non-agitated and shaking condition of fermentation respectively. The results show that the maximum yeast cell biomass concentration was reached after 40 hours of fermentation. The R^2 values between predicted and experimental values of cell mass under the non-agitated and agitated condition of SSF were found as 0.972 and 0.983 respectively as shown in Table 4.7.

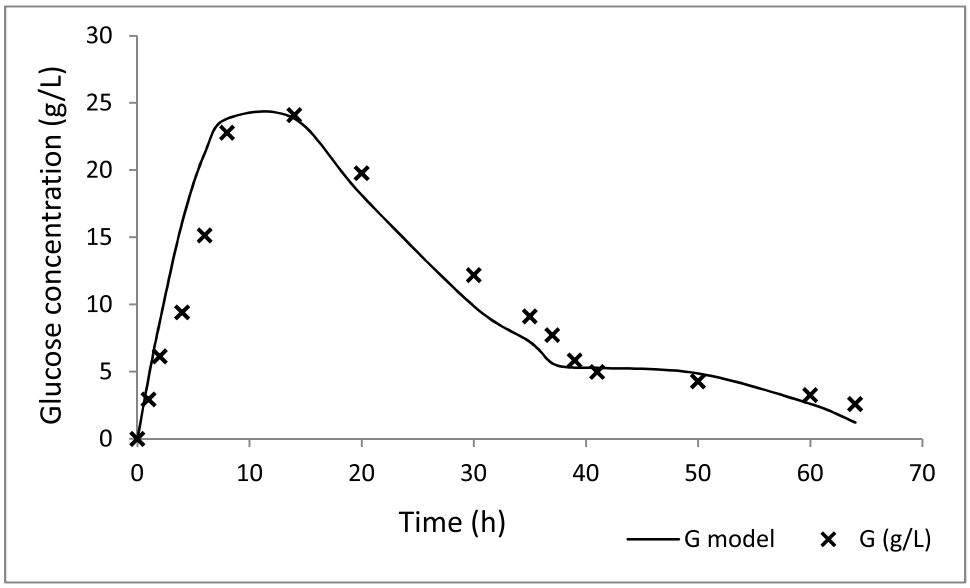

Fig. 4.58: Profile of predicted (lines) and experimental (×) glucose (G) concentration during the simultaneous Saccharification and fermentation (SSF) process under the non-agitated condition

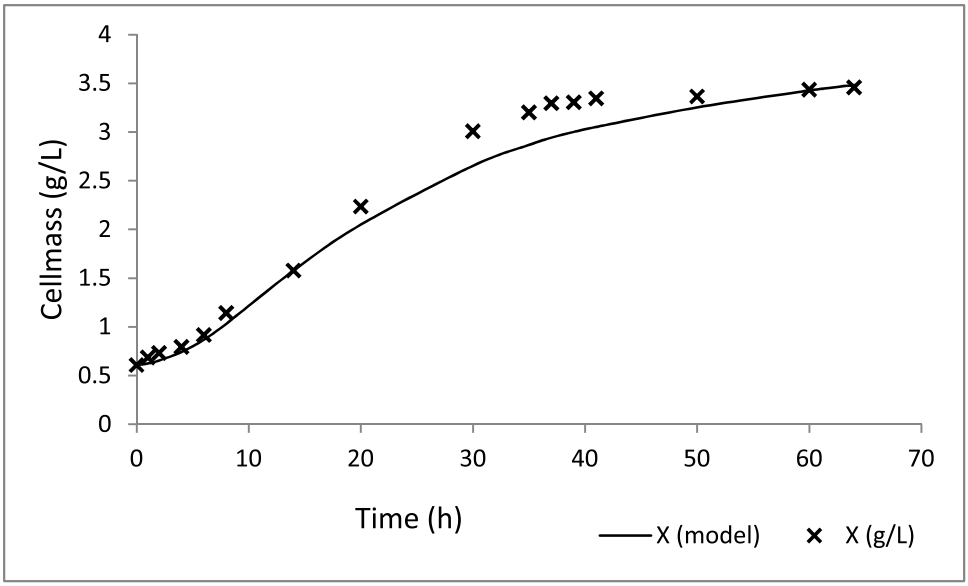

Fig. 4.59: Profile of predicted (lines) and experimental (×) cell mass concentration during the simultaneous Saccharification and fermentation (SSF) process under the non-agitated condition

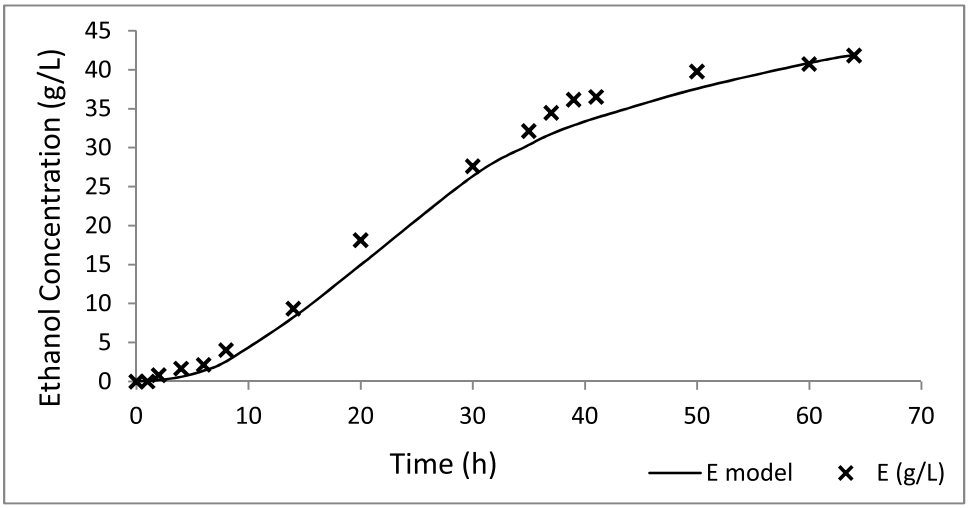

Fig. 4.60: Profile of predicted (lines) and experimental (×) bioethanol (E) concentration during the simultaneous saccharification and fermentation (SSF) process under the non-agitated condition

Table 4.7: Coefficient of determination (R^2) for different models

Predicted models for	Models	R^2- values	
		Non-agitated	Agitated
Carbohydrate	$-\frac{dS}{dt} = V_m \frac{S}{k_m + S}$	0.998	0.997
Glucose	$\frac{d[G]}{dt} = 1.11\, V_m \frac{S}{k_m + S} - \left[\frac{1}{Y_{P/S}}\frac{dP}{dt} + \frac{1}{Y_{X/S}}\frac{dX}{dt} + m_s X\right]$	0.914	0.935
Cell mass	$\frac{dX}{dt} = \mu_m \frac{G}{k_s + G} X$	0.972	0.983
Ethanol	$\frac{dP}{dt} = q_m \frac{G}{k_s + G} X$	0.988	0.984

The predicted and experimental values of ethanol concentration under the non-agitated and agitated condition of fermentation are shown in Figure 4.60 and 4.65 respectively. In non-agitated fermentation condition, the predicted values of ethanol were slightly lower than experimental values during exponential phase. In shaking condition of fermentation, the predicted values of ethanol were slightly greater than experimental values during exponential phase. However, at the end of the SSF process, the experimental value of ethanol concentration was higher than the predicted values. Table 4.7 shows that the R^2 value between predicted and experimental values of ethanol concentration was found as 0.988 and 0.984 under non-agitated and shaking condition of fermentation respectively. It was observed that R^2 values for various models were found greater than or near to 0.95 except for glucose concentration. Thus, this can be concluded that these models can predict experimental values with greater accuracy.

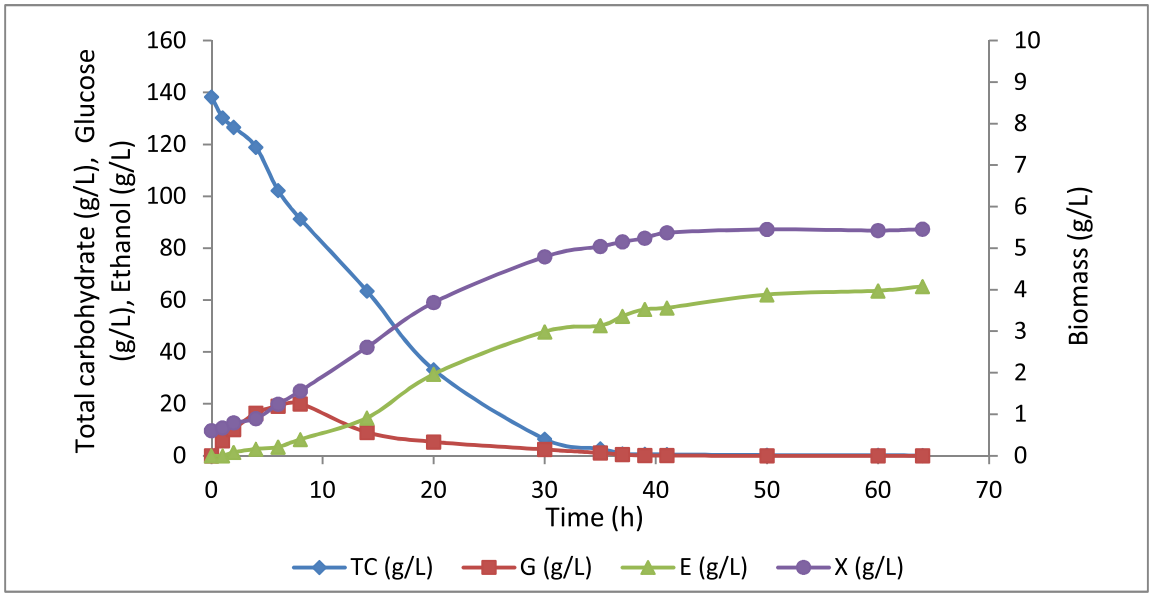

Fig. 4.61: The concentration profiles of glucose (*G*), starch (*S*) and ethanol (*E*) and yeast cell mass (*X*) during SSF under the agitated condition

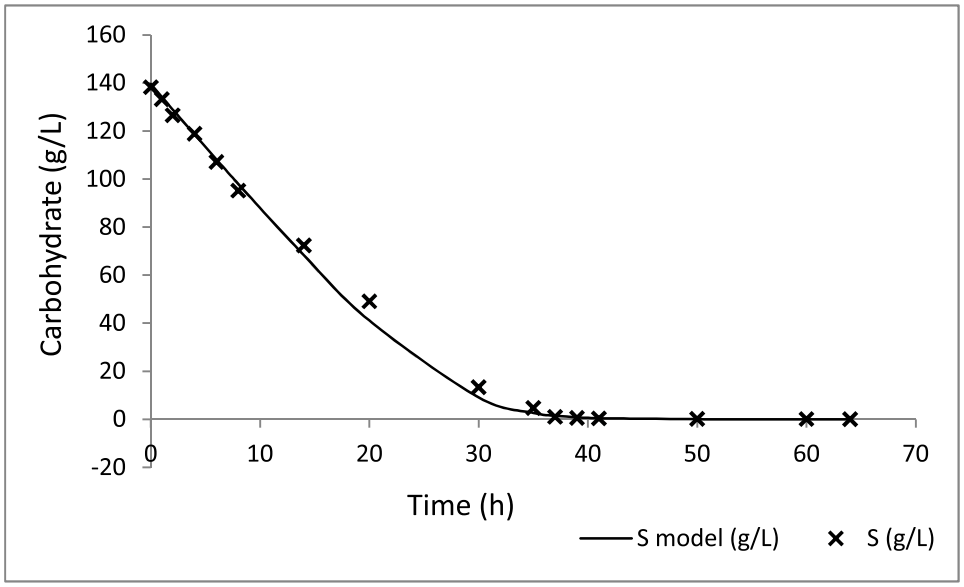

Fig. 4.62: Profile of predicted (lines) and experimental (×) carbohydrate depletion during the simultaneous saccharification and fermentation (SSF) process under the agitated condition

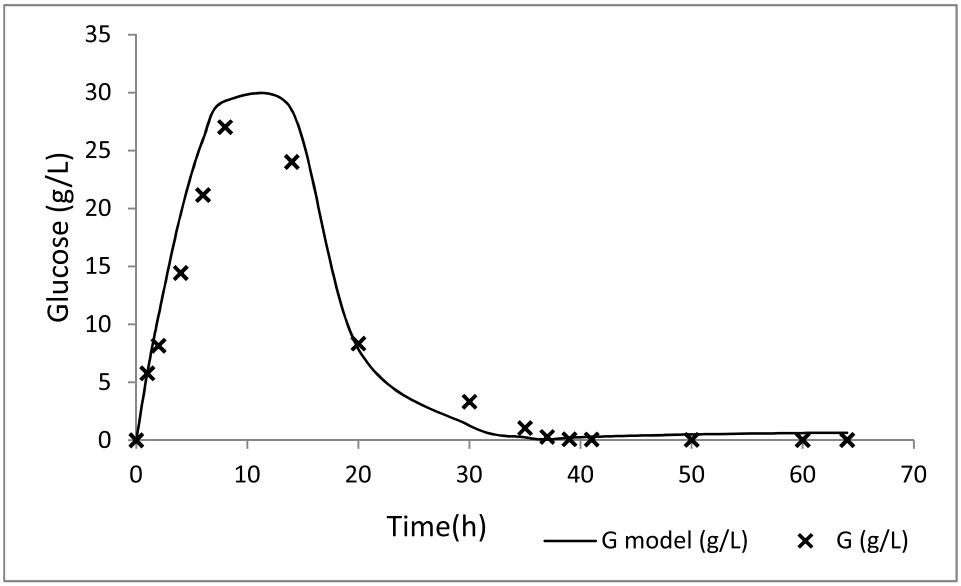

Fig. 4.63: Profile of predicted (lines) and experimental (×) glucose (G) concentration during the simultaneous saccharification and fermentation (SSF) process under the agitated condition

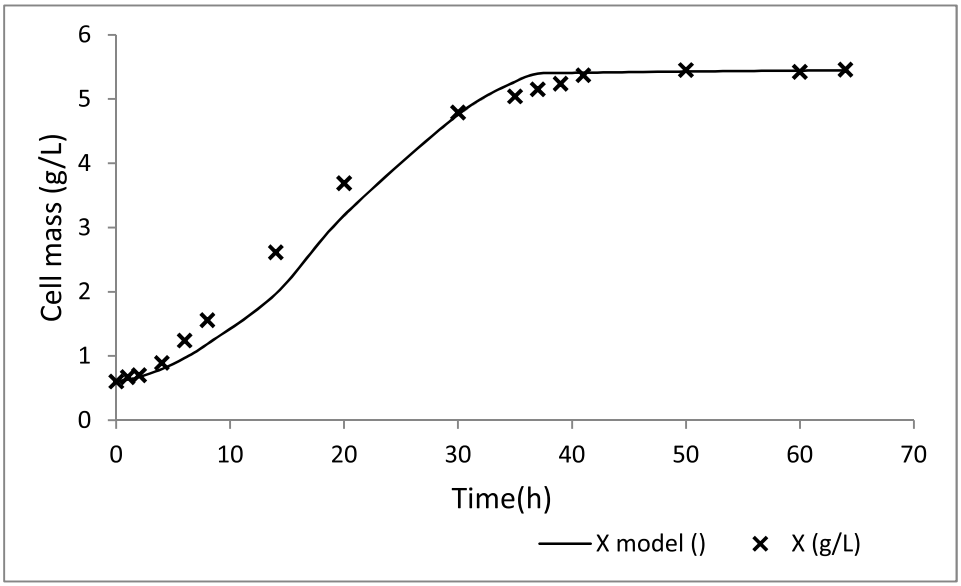

Fig. 4.64: Profile of predicted (lines) and experimental (×) cell mass concentration during the simultaneous saccharification and fermentation (SSF) process under the agitated condition

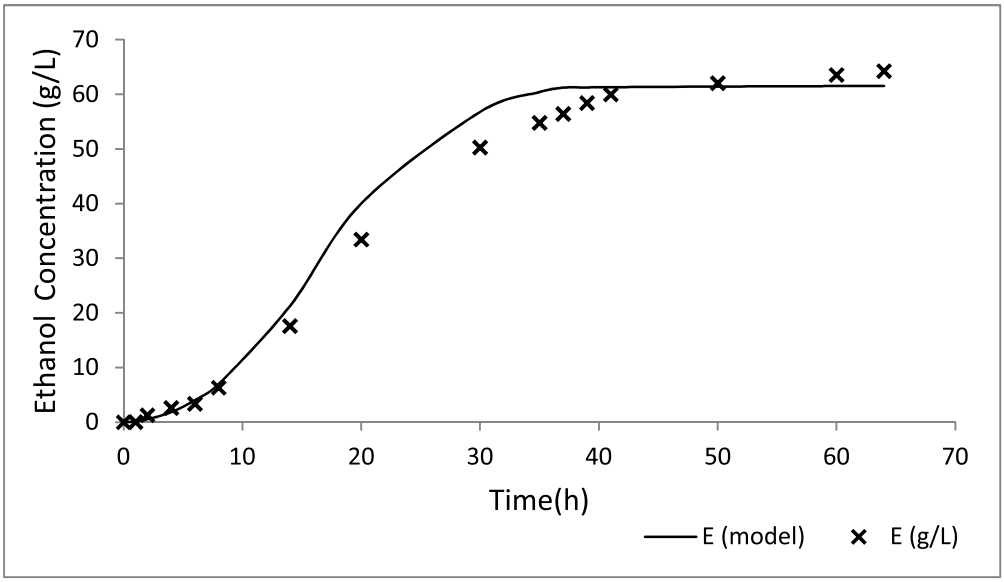

Fig. 4.65: Profile of predicted (lines) and experimental (×) bioethanol (E) concentration during the simultaneous saccharification and fermentation (SSF) process under the agitated condition